AD-A111 149 RCA LABS PRINCETON NJ F/G 18/8
EFFECTS OF RADIATION ON OXIDE MATERIALS.(U)
NOV 81 B W HUGHES, J H THOMAS DAA639-77-C-0159
UNCLASSIFIED PRRL-79-CR-12 HDL-CR-79-159-1 NL

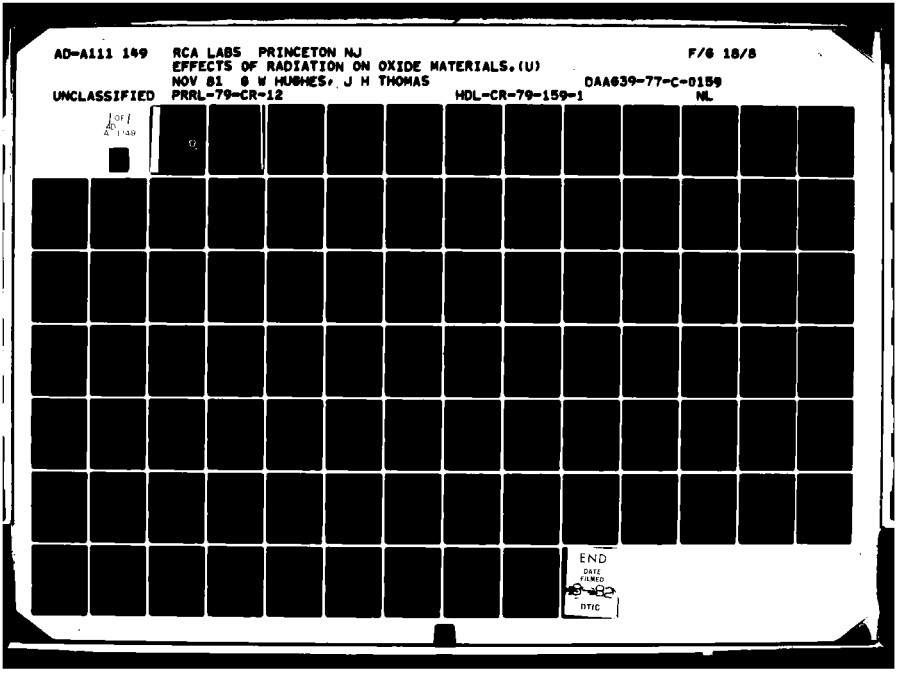

HDL-CR-79-159-1

November 1981

(12) LEVEL II

EFFECTS OF RADIATION ON OXIDE MATERIALS

by Gary W. Hughes and John H. Thomas III

Prepared by

RCA Laboratories
Princeton, NJ 08540

Under contract

DAAG39-77-0159
C

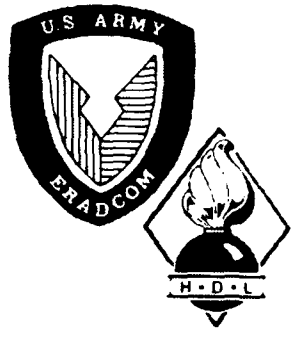

U.S. Army Electronics Research
and Development Command
Harry Diamond Laboratories
Adelphi, MD 20783

The findings in this report are not to be construed as an official Department of the Army position unless so designated by other authorized documents.

Citation of manufacturers' or trade names does not constitute an official indorsement or approval of the use thereof.

Destroy this report when it is no longer needed. Do not return it to the originator.

UNCLASSIFIED

SECURITY CLASSIFICATION OF THIS PAGE (When Data Entered)

REPORT DOCUMENTATION PAGE	READ INSTRUCTIONS BEFORE COMPLETING FORM
1. REPORT NUMBER: HDL-CR-79-159-1	2. GOVT ACCESSION NO.: AD-A111 149
3. RECIPIENT'S CATALOG NUMBER	
4. TITLE (and Subtitle): EFFECTS OF RADIATION ON OXIDE MATERIALS	5. TYPE OF REPORT & PERIOD COVERED: FINAL REPORT (9-26-77 to 9-25-78)
	6. PERFORMING ORG. REPORT NUMBER: PRRL-79-CR-12
7. AUTHOR(s): Gary W. Hughes and John H. Thomas III	8. CONTRACT OR GRANT NUMBER(s): DAAG39-77-C-0159
9. PERFORMING ORGANIZATION NAME AND ADDRESS: RCA Laboratories, Princeton, NJ 08540	10. PROGRAM ELEMENT, PROJECT, TASK AREA & WORK UNIT NUMBERS
11. CONTROLLING OFFICE NAME AND ADDRESS: Defense Nuclear Agency, Washington, DC 20305	12. REPORT DATE: November 1981
	13. NUMBER OF PAGES: 89
14. MONITORING AGENCY NAME & ADDRESS (if different from Controlling Office): Harry Diamond Laboratories, 2800 Powder Mill Rd., Adelphi, MD 20783	15. SECURITY CLASS. (of this report): Unclassified
	15a. DECLASSIFICATION/DOWNGRADING SCHEDULE: N/A

16. DISTRIBUTION STATEMENT (of this Report)

Approved for public release; distribution unlimited.

17. DISTRIBUTION STATEMENT (of the abstract entered in Block 20, if different from Report)

18. SUPPLEMENTARY NOTES

19. KEY WORDS (Continue on reverse side if necessary and identify by block number)

Radiation-hardened SiO_2
MOS
Hole traps
Mobile-ion instability
Slow-trapping instability
Nonstoichiometric SiO_2
Hydrogen in SiO_2

20. ABSTRACT (Continue on reverse side if necessary and identify by block number)

Dry and wet(pyrogenic steam)-grown thermal oxides on (100) silicon were made for an investigation of the radiation sensitivity of MOS devices. Oxides were grown under conditions known to produce state-of-the-art hardened oxides as well as very soft oxides. MOS capacitors were fabricated with thin semi-transparent and thick aluminum gates

DD FORM 1 JAN 73 1473

UNCLASSIFIED

SECURITY CLASSIFICATION OF THIS PAGE (When Data Entered)

20.

for irradiation with 10.2-eV vacuum ultraviolet (VUV) photons and 1-MeV electrons, respectively.

Electrical measurements were made on MOS capacitors to determine trapped-charge density, charge transport, and thermal-trap depth, using high frequency and quasi-static CV, triangular voltage sweep (TVS), and thermally stimulated current (TSC) techniques. Preirradiation measurements showed that oxides contained both sodium and potassium mobile ions in concentrations ranging from 3.5×10^{10} to 1.5×10^{12} cm^{-2}. Capacitors with the highest concentrations (and, incidentally, the highest degree of radiation hardness) had ions distributed in a laterally nonuniform manner. Thin-metal MOS capacitors on wet oxides were shown to have a slow-trapping instability. A characterization of this instability has shown it to be caused by the temperature assisted field emmission of electrons from neutral traps.

TSC measurements taken on irradiated capacitors to characterize the thermal-energy trap spectra gave varied results. Dry-oxide TSC spectra show a gradual increase in TSC current between 300 and 600 K with no pronounced structure. Wet-oxide capacitors exhibit two different types of behavior, depending on whether preirradiation thermal behavior is dominated by slow trapping or by mobile ions. Mobile-ion-dominated capacitors show postirradiation TSC spectra with distinct peaks at 335 and 585 K; peaks at these temperatures are believed to indicate the presence of sodium and potassium ions, respectively. No increase in mobile-ion density is observed. It is concluded that irradiation and/or hole flux can move mobile ions from the aluminum to the silicon interface. Capacitors with slow-trapping problems exhibit a two-stage hole-trapping process with an intermediate state unaffected by the field-emission center and a final state whose energy depends upon the occupancy of the field-emission center.

Analytical measurements of interface stoichiometry and impurity profiles were done by the use of ion-scattering spectroscopy (ISS), x-ray photoelectron spectroscopy (XPS), and secondary-ion mass spectroscopy (SIMS). XPS measurements showed the presence of interfacial nonstoichiometric silicon in all types of oxides. The intermediate-state density thus measured is larger in hardened than in soft oxides. We suggest that these states may somehow compensate for the disorder that is probably associated with hole traps. The analysis of impurity profiles shows that the SIMS technique is capable of measuring sodium and hydrogen at low levels. A hydrogen profile in a 1100°C steam oxide shows an as-grown concentration of hydrogen of 8×10^{19} cm^{-3}.

PREFACE

This final report, prepared by RCA Laboratories, Princeton, NJ, under contract DAAG39-77-C-0159, describes work performed principally in the Solid State Technology Center, D. E. O'Connor, Director.

The Project Scientist is G. W. Hughes. Ion-scattering spectroscopy (ISS) measurements were done by W. L. Harrington, secondary-ion mass spectrometry (SIMS) measurements by C. W. Magee, and x-ray photoelectron spectroscopy (XPS) measurements by J. H. Thomas III, all of RCA Laboratories. Device processing and radiation testing were performed with the assistance of R. W. Snedeker and F. A. Taft, Jr.

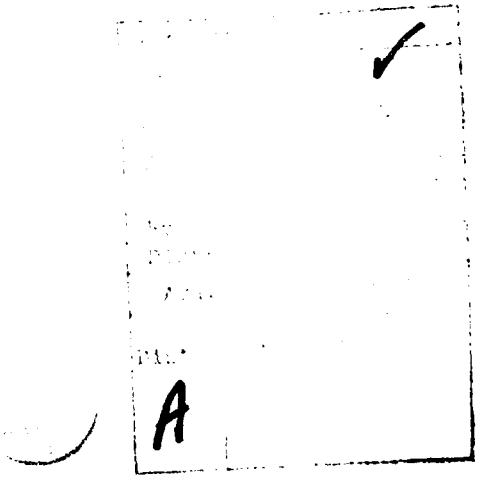

Blank

TABLE OF CONTENTS

TABLE OF CONTENTS (Continued)

LIST OF ILLUSTRATIONS

LIST OF ILLUSTRATIONS (Continued)

LIST OF TABLES

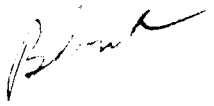

1. INTRODUCTION

This report describes the results of radiation effect studies on wet- and dry-grown thermal SiO_2 MOS oxides. These oxides were grown at RCA Laboratories in dedicated radiation-hardened wafer fabrication furnaces for use in this study as well as in other studies carried out by Harry Diamond and Jet Propulsion Laboratories. The purpose of all these studies was to learn more about the nature of the radiation damage mechanisms in thermal SiO_2 MOS devices by the use of identical samples fabricated by a single supplier. Both electrical and chemical measurements were carried out on these samples. Because chemical analysis of oxides is not nearly as sensitive as electrical measurements for detecting species with the densities of typical hole-traps in hard oxides, oxides were grown deliberately hard and soft for both wet- and dry-oxide types. Oxidized wafers were not metallized for chemical analysis. For electrical analysis, MOS capacitors were formed by evaporation of aluminum. Although many of the radiation-hardened device processes are now based exclusively on polysilicon-gate technology, no polysilicon-gate devices were studied. A broad foundation of fundamental research in radiation-hardened oxides exists for aluminum-gate structures, whereas very little has been done for polysilicon-gate devices.

The principal electrical measurements described here are thermally stimulated current (TSC) measurements of irradiated MOS capacitors. These measurements were designed to reveal the thermal "signature" of trapped holes in the various fabricated oxides. The assumption is that since the radiation response of hard and soft oxides is so significantly different, the thermal detrapping of these holes might reveal something about the nature of the hold traps themselves. The chemical analysis experiments were designed to measure differences in the stoichiometry, chemical bonding, and impurity profiles of the various oxides. Here we used tools such as ion-scattering spectrometry (ISS) to measure stoichiometry, x-ray photoelectron spectroscopy (XPS) to measure chemical bonding, and secondary-ion mass spectrometry (SIMS) to measure impurity profiles.

Section 2 describes the preparation of the samples and summarizes the pertinent fabrication and radiation data for cross referencing in reading of the report. Section 3 explains briefly the electrical measurement techniques used to characterize these samples, going into more detail for the more unconventional ones. A comparison of irradiation techniques with respect to absorbed dose and dose rate is also given. Section 4 describes the preirradiation measurements we made on these samples, especially the characterization of slow trapping and the mobile ions some of them contain. Section 5 details the postirradiation electrical measurements, especially TSC measurements of the wet oxides, which provided some very interesting information. Section 6 presents the analytical measurements we made to analyze these oxides and the conclusions that we arrived at concerning the chemical nature of the oxides as it relates to hole trapping and radiation hardness. Section 7 presents a summary and some general conclusions.

2. SAMPLE PREPARATION

All samples used in this study were fabricated from Monsanto 2-in.-diameter Czochralski-grown (100) silicon wafers, with n-and p-type doping of 5- to 10-Ω-cm resistivity. Before oxidation, wafers to be used in vacuum ultraviolet (VUV) irradiation experiments, and therefore not mounted on TO-5 headers, received either n^+ or p^+ diffusion on the back surface of the wafer to facilitate the fabrication of ohmic back contacts. These diffusions were done by a doped-oxide process in which the front surface of the wafer is covered by a deposited oxide to mask it from the diffusion. After doped-glass deposition the dopant is driven in at 1050°C and the glass is removed. Before oxidation all wafers received a standard cleaning treatment which consists of a hydrofluoric acid dip followed by cleaning in an organic-impurity removal solution (NH_4OH, H_2O_2, and H_2O) and a metallic-impurity removal solution (HCl, H_2O_2, and H_2O). Wafers were rinsed to 15-MΩ resistivity in deionized water, rinsed in hot distilled water, and then dried in hot clean air.

2.1 Wet Oxides

Wet oxidation was done by the so-called pyrogenic process whereby hydrogen is burned in the presence of oxygen inside a furnace tube to create water. This technique has the advantages of being easy to control and of not compromising the purity of the aqueous product by impurities leached from heated quartz vessels as occur in steam oxidation. As a standard procedure for both wet and dry oxidation, the furnace tube is cleaned overnight in an azeotropic HCl steam solution. The tube is then purged with dry oxygen for 2 hours before oxidation begins. All oxidations were done in a 3-in.-diameter polysilicon furnace tube contained within a silicon carbide liner.

Deciding on a particular oxidation procedure to follow for growing hard and soft oxides was mainly a matter of using what is generally accepted as a "hardened-oxide process" for the hard oxides and modifying the oxidation or anneal temperature to produce a soft oxide.

Although this study assumes that we do not yet know why a particular oxide is hard, there are some generally accepted notions as to how hardened oxides can be fabricated. Some of the early hard-oxide work, particularly that done by Aubuchon,[1] followed the rule that oxides will be hard if they are grown in dry O_2 at about 1000°C in HCl-precleaned furnace tubes. Other studies have confirmed this strong temperature dependence,[2,3] although we have shown that it is not as strong as it was thought to be.[4] The dry-oxide samples grown for this study again support this viewpoint. Thus we see that both impurities

---

[1] K. Aubuchon, IEEE Trans. Nucl. Sci. NS-18, 117 (1971).

[2] G. Derbenwick and B. Gregory, IEEE Trans. Nucl. Sci. NS-22, 2151 (1975).

[3] G. W. Hughes and R. J. Powell, "Radiation and Charge Transport in SiO_2," Final Report prepared under Contract N00014-74-C-0185 for Office of Naval Research, May 1976.

[4] G. W. Hughes, "Radiation and Charge Transport in SiO_2," Final Report prepared under Contract N000A-74-C-0185 for Office of Naval Research, Feb. 1977.

and oxidation kinetics are thought to play a role in radiation hardening.

Because of the requirements of both factory production and the low-leakage current in silicon-on-sapphire (SOS) technology, a radiation-hardened wet-oxidation process was developed throughout the industry. At RCA this process has evolved to the "recipe" shown in table 1. This yields an oxide of approximately 650-Å thickness. The effectiveness of an added in situ dry-oxidation step is a matter of controversy. However, it probably does not hurt the radiation hardness of the oxide and will most likely remain in the process for some time to come.

In an investigation of this sort one would like to have a high degree of control over the process. However, although we believe that impurities may play a role in radiation hardening, they are not completely under our control. We can, however, control the oxidation and annealing kinetics, and if they do have a first-order effect on radiation hardening we will be able to produce hardened and soft oxides by varying the oxidation and anneal conditions.

TABLE 1. SUMMARY OF FABRICATION PROCEDURES FOR WET-OXIDE PROCESS

	Type of oxide	
Procedure	Hardened wet	Soft wet
Pyrogenic steam Oxidation (2 L/min O_2, 1.2 L/min H_2)	900°C, 45 min	900°C, 45 min
Dry oxidation	900°C in situ, 30 min	900°C in situ, 30 min
Nitrogen anneal	900°C in situ, 30 min	1150°C, 30 min
Metallization and 450°C sinter (forming gas or nitrogen)	15 min	15 min

For wet oxides it has been observed that high-temperature anneals produce soft oxides. We have grown soft wet oxides for this investigation by changing the anneal temperature in the wet-oxide process from 900 to 1150°C. This process is also shown in table 1.

2.2 Dry Oxides

Hardened dry oxides were grown in a polysilicon furnace tube at 1000°C with no subsequent anneal. This is the commonly accepted method of producing radiation-hardened dry SiO_2. Table 2 summarizes the oxidation process used to make both the hard and the soft dry SiO_2.

TABLE 2. SUMMARY OF FABRICATION PROCEDURES FOR DRY-OXIDE PROCESS

	Type of oxide	
Procedure	Hardened dry	Soft dry
Dry oxidation	1000°C, 110 min	1150°C, 15 min
No anneal	--	--
Metallization and 450°C sinter (forming gas or nitrogen)	15 min	15 min

Again, since it is widely believed that oxidation kinetics have a first-order effect on hardness, we tried to grow soft dry oxides by oxidizing at 1150°C. As the radiation data in table 3 (see section 2.3) show, the oxides thus obtained were not nearly as soft as anticipated; this confirmed our earlier observations on the lack of a strong temperature dependence of the radiation tolerance of dry SiO_2.

2.3 Metallization

MOS capacitors employed in these experiments were of two types. Thick-metal capacitors mounted on gold-plated TO-5 headers were used for high-energy irradiation experiments. Thin-metal capacitors in wafer form were used for VUV experiments. All metallization was provided by an induction-heated crucible, a source that has been established as low in alkaline impurities and free from radiation.

Thick-metal capacitors were formed by the photolithographic definition of 12,000 Å of aluminum (Al) into 0.040-in. dots. The back surface of the wafer was etched free of SiO_2. After sintering, the individual capacitors were diced into pellets and then mounted with a gold eutectic on the gold-plated TO-5 headers at 400°C in forming gas. For n-type silicon, a Au/Si/Sb eutectic was used to dope the pellet backside for good ohmic contacts; for p-type silicon, a Au/Si eutectic provided the necessary ohmic contact.

Thin-metal capacitors were formed by evaporating 20 Ω/□ of Al through a Be-Cu shadow mask to form 0.040-in.-diameter MOS dots approximately 100-200 Å thick. The back surface of these wafers (which contained either n^+ or p^+ diffusions) was previously etched free of SiO_2 and then metallized completely with 12,000 Å of Al. All wafers, both thick- and thin-metal capacitor types, were sintered at 450°C for 15 min in either a forming gas or nitrogen ambient. This is specified in table 3.

The use of a forming gas sinter has been variously described as both a cause and a cure for the many problems that beset MOS devices. Specifically, it has been said to be beneficial in reducing the density of interface states in MOS devices.[5,6] However, it has also been accused of increasing the severity of the so-called "slow-trapping" instability in MOS devices.[7] The samples we have fabricated for this study were exposed to either a forming gas sinter or a nitrogen sinter (see table 3). Most of the data reported here refer to samples fabricated with a forming gas sinter. Some of these samples do have a severe slow-trapping instability problem. However, since this is limited exclusively to thin-metal capacitors, it appears to be more a function of external impurities than of sintering ambinet. This is discussed in more detail in section 4.1.

---

[5] B. E. Deal, J. Electrochem. Soc. 121(6), 198C (1974).

[6] B. E. Deal, "Charge Effects and Other Properties of the Si/SiO_2 Interface: The Current Understanding," Proc. Third Int. Symp. Silicon Materials Science and Technol. 1977, p. 276.

[7] A. K. Sinha and T. E. Smith, Solid-State Electron. 21(3), 531 (1978).

TABLE 3. WAFER FABRICATION AND RADIATION DATA

DRY-OXIDE WAFERS

Lot no.	ΔV_{FB}(volts) at 10^6 rad		Sinter	Wafers with thin metal	Oxide thickness
	Hardened	Soft			
12067(n)	3.4	--	N_2	C,D	804
12067(p)	2.7	--	N_2	H,I	
12167(n)	2.0	--	N_2	E,F	745
12167(p)	?	--	N_2	Q,R	
01268(n)	---	?	N_2	C,D	739
01268(p)	---	?	N_2	I,J	
05258(n)	2.0	--	N_2	A,B	670
05258(p)	?	--	N_2	H	
05268(n)	---	3.0	N_2	A,B	696
05268(p)	---	6.0	N_2	H	
11088(n)	2.8	--	FG	H,I	716
11088(p)	?	--	FG	L,M	
11168(n)	---	3.6	FG	H,I	687
11168(p)	---	?	FG	L,M	

WET-OXIDE WAFERS

03068-A-D(n)	2.8	--	N_2	None	907
03068K(p)	5.4	--	N_2	None	
03068F-J(n)	---	41	N_2	None	953
03068L(p)	---	26	N_2	None	

TABLE 3. WAFER FABRICATION AND RADIATION DATA (Continued)

Lot no.	ΔV_{FB}(volts) at 10^6 rad: Hardened	Soft	Sinter	Wafers with thin metal	Oxide thickness
04118(n)	3.0	0-	N_2	D,E	850
04118(p)	?	--	N_2	K,L	
04138(n)	---	34	N_2	D,E	912
04138(p)	---	?	N_2	K,L	
06128(n)	1.2	--	FG	H,I	653
06128(p)	2.5	--	FG	K,L	
06168(n)	---	34	FG	H,I	665
6168(p)	---	?	FG	K,L	

2.4 Summary of Fabrication and Radiation Data

Table 3 is a tabulation of all of the oxide lots produced for this study. Included in this list is the lot number; the flatband shift after a 10^6-rad dose of 1-MeV electrons; the sample type tested (n or p); the sintering ambient, N_2, or forming gas (FG); the letter identifiers for this thin-metal-capacitor wafers; and the oxide thickness. The radiation data are for 1-MeV electrons at a dose rate of 10^4 rad/s. These flatband voltage shifts should be "derated" by a multiplying factor of about 0.6 to estimate the test results in a typical ^{60}Co source with a dose rate of 250 rad/s. The wafer number consists of five digits followed by a letter (the thin-metal capacitors are identified by the letters shown in table 3). The number is essentially the date of fabrication. For example, sample 06128H(n) is an n-type wafer with semitransparent thin-metal capacitors fabricated on June 12, 1978.

3. ELECTRICAL MEASUREMENT TECHNIQUES

Electrical measurements performed on these samples consisted of standard 1-MHz high-frequency capacitance-voltage (HFCV) measurements, quasi-static capacitance-voltage (QSCV) measurements, triangular voltage sweep (TVS) measurements (really QSCV measurements at elevated temperatures), and thermally stimulated current (TSC) measurements. As both HFCV and QSCV measurements are familiar to most workers in the MOS physics area,[8,9] we will not dwell on them here.

3.1 Triangular Voltage Sweep (TVS)

TVS measurements are used to measure the motion of mobile ions in MOS capacitors, but there is some disagreement as to how they should be interpreted.[10,11] The basic measurement scheme and typical results are shown in figure 1. The measurement consists of raising an MOS capacitor to an elevated temperature (typically 250-300°C) and sweeping a voltage on the gate at a constant rate α. As shown in the figure, the current through the capacitor is plotted as a function of gate voltage. When no mobile ions are present, the current will follow the dashed portion shown in the region around zero bias. This is the QSCV curve at this particular temperature. In the presence of mobile ions, if the sweep rate α is low enough for the ions to be in quasi-thermal equilibrium, the mobile ion density Q_M has been shown to be

$$Q_M = \frac{1}{\alpha} \int_{-V_D}^{V_D} I_T(v)dv - \int_{-V_D}^{V_D} I_c(v)dv \qquad (1)$$

where $I_T(v)$ is the total current measured and $I_c(v)$, the current measured due to the MOS capacitance.[10] The ion density is, therefore, proportional to the area between the two curves, shown by the shaded area in figure 1.

---

[8] S. R. Hofstein and G. Warfield, Solid-State Electron. 8, 321, (1965).
[9] M. Kuhn, Solid-State Electron. 13, 873 (1970).
[10] M. Kuhn and D. J. Silversmith, J. Electrochem. Soc. 118(6), 966 (1971).
[11] N. J. Chou, J. Electrochem. Soc. 118(4), 601 (1971).

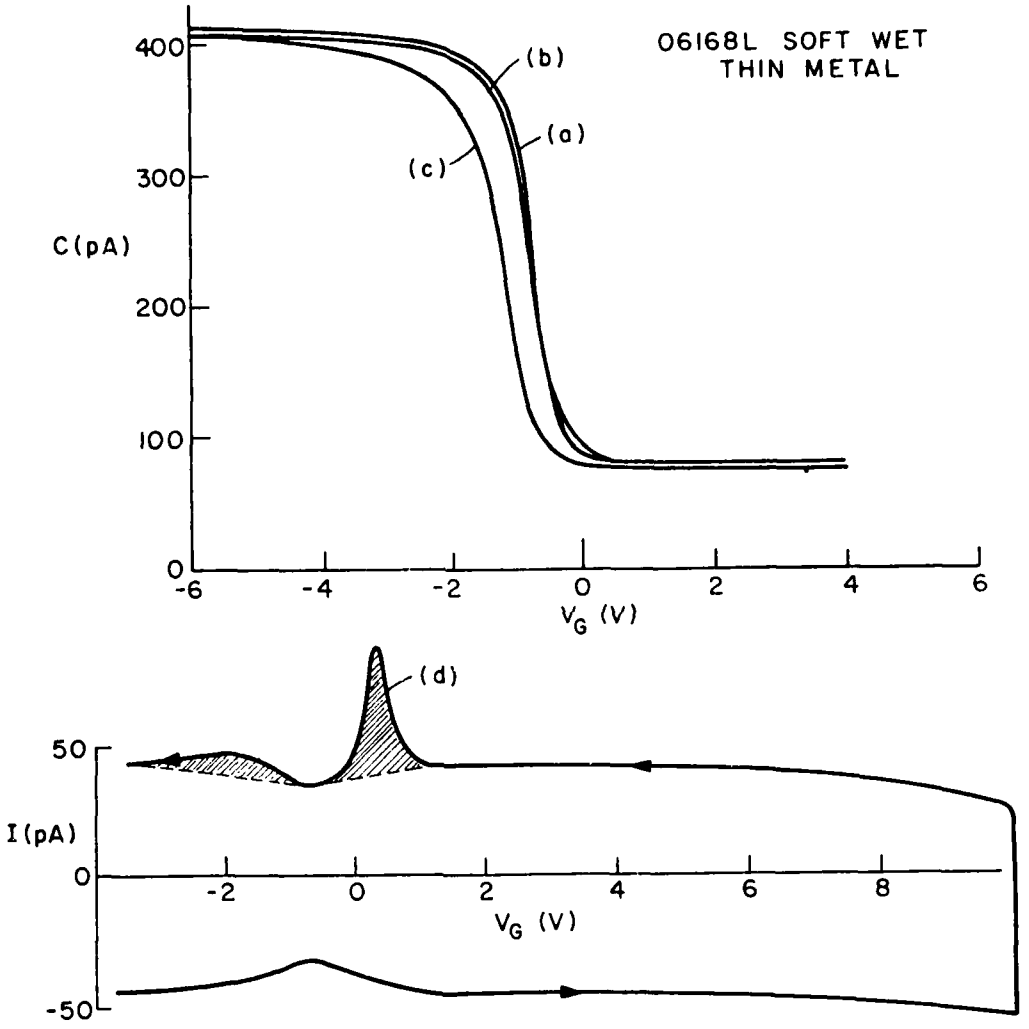

Figure 1. CV and TVS measurements on sample 06168L. (a) Initial CV curve; (b) CV curve after ⊕ → ⊖ sweep; (c) CV curve after ⊖ → ⊕ sweep; (d) TVS curve: α = 0.1 V/s, T = 300°C. Total mobile-ion concentration $N_M = 1.8 \times 10^{11}$ cm^2.

Kuhn has argued that this technique is more accurate than the conventional method of measuring CV shifts after bias-temperature stressing because it is largely independent of MOS oxide charge and interface states.[10] However, there are several caveats to be observed if this is to hold true. One is that the ions must be in quasi-equilibrium during the sweep. This requires low voltage-sweep rates and/or high temperatures. Derbenwick, however, has shown that potassium is an important mobile ion in SiO_2 which is not in quasi-equilibrium under the conditions normally used to measure sodium contamination.[12] A second warning is that the temperature must not be so high that electrode reactions become important. Chou believes that this may take place at and above 350°C in SiO_2/Al capacitors.[11] (Derbenwick, on the other hand, claims that the phenomenon observed by Chou might actually have been potassium motion, and that electrode reactions are not really important at this temperature.[12]) To this list we must add a third: that there must be no charge injection or detrapping occurring during the portion of the voltage sweep where mobile ions are contributing to the current.

At temperatures above 350°C and positive bias a significant dc leakage current exists in the thin MOS capacitors we measured, an effect that we believe to be caused by the Fowler-Nordheim tunneling of electrons from the silicon to the SiO_2. This is evident in figure 1 for $V_G > 6$ volts. However, as shown here as well, the leakage is negligible for $V_G < 2$ volts, the region where ion current becomes significant. The problem of injection or detrapping is important in our irradiated samples, since there can be trapped holes and/or slow-trapping states capable of contributing to the measured current. This will be discussed in section 5, in connection with TVS measurements on irradiated devices.

3.2 Thermally Stimulated Currents (TSC)

The technique of using thermally stimulated current and thermally stimulated luminescence (or thermoluminescence) has been

[12] G. F. Derbenwick, J. Appl. Phys. 48(3), 1127 (1977).

applied for years to the study of the trapping levels of electrons in insulators. However, the theory of TSC was originally developed for only a few very simple cases involving discrete trapping levels. A general treatment involving traps that are arbitrarily distributed throughout the bandgap of the insulator was not amenable to analytical solution. Consequently, in most of the early work, it was difficult to correlate theory with experiment.[13] In recent years Simmons has shown that most of these problems could be eliminated if analysis and experiment were confined to high-field conditions in the insulator so that electrons and holes could not recombine.[14] In fact Simmons and coauthors have shown that under high-field conditions the shape of the TSC characteristics is a direct image of the energy distribution of occupied traps in the insulator bandgap. Because the insulators have a high dielectric strength and are relatively thin, high-field conditions are easily met in MOS devices. The one flaw in Simmons's technique is that it cannot distinguish between trapped electrons and holes. As the temperature is raised, holes trapped near the valence band will be emitted at the same temperature as those electrons that are trapped at an equal energy below the conduction band. Thus the electron and hold trap spectra will be superimposed upon one another. Fortunately, for irradiated SiO_2 we are fairly confident that holes have a much larger capture cross section than have electrons and thus are trapped in substantially greater numbers.[15-17] Any TSC spectra measured after irradiation should consist ideally of only detrapped holes. In practice the presence of mobile ions and/or a slow-trapping instability adds

---

[13] P. Kelley and P. Braunlick, Phys. Rev. B 1, 1587 (1970).
[14] J. G. Simmons, G. W. Taylor, and M. C. Tam, Phys. Rev. B 7(8), 3714 (1973).
[15] D. J. DiMaria, in The Physics of SiO_2 and Its Interfaces, ed. by S. T. Pantelides (Pergamon Press, New York, 1978), p. 160.
[16] G. W. Hughes, "Radiation Effects on the Electrical Properties of MOS Device Materials," Final Rept. Prepared under Contract DAAG39-76-C-0088 for Defense Nuclear Agency, Feb. 1978.
[17] R. J. Powell and G. F. Derbenwick, IEEE Trans. Nucl. Sci. NS-18(6), 10 (1971).

additional components of current that must be dealt with. This will be discussed in section 3.3.

The theory of high-field TSC has been well developed by Simmons and coworkers and will not be reported here.[14] Their results assume both holes and electrons trapped uniformly throughout the insulator. For the case in which we are interested, only holes are trapped, and we will assume that all of them are trapped very close to the Si/SiO_2 interface. (This location asymmetry has been verified by several etch-off experiments.[17,18])

The basic technique of TSC measurement is illustrated in figure 2. A constant bias is applied to the MOS sample to establish high-field conditions at room temperature. The sample is then heated at a constant rate β so that the sample temperature is given by

$$T = \beta t + T_o \tag{2}$$

where T_o is the starting temperature sweep rate and t is time. The current measured is then plotted as a function of temperature and yields some spectrum perhaps like that shown in the figure. For trapped holes at the Si/SiO_2 interface the spectrum is a direct map of the density of trapped holes $N_p(E)$ as a function of energy, if the following conversions are used[14]:

$$N_p(\Delta E) = \frac{J_p(T)}{qLD\beta} \tag{3}$$

where J_p is the measured hold-current density, q is the electronic charge, L is the oxide thickness, β is the sweep rate,

$$D = (2.30^4 \times 10^{-4} \log_{10} \frac{\nu}{\beta} + 3.84 \times 10^{-4}) - \frac{0.018}{T} \tag{4}$$

[18] R. J. Powell and G. W. Hughes, "Radiation and Charge Transport in SiO_2," Final Rept. prepared under Contract N00014-74-C-0185 for Office of Naval Research, 31 Jan. 1975.

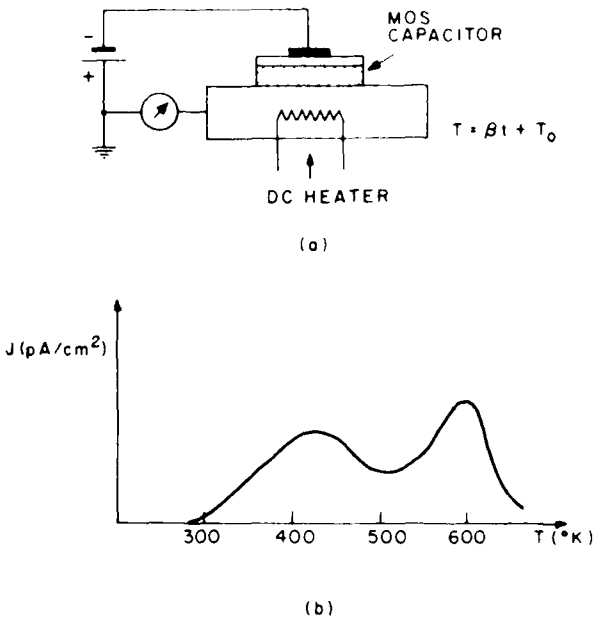

Figure 2. Thermally stimulated current (TSC) measurement technique. (a) Schematic of TSC apparatus; (b) typical current-vs-temperature plot for linear temperature sweep.

and

$$\Delta E = E_{tp} - E_v = T(1.92\times10^{-4} \log_{10} \frac{\nu}{\beta} \quad 3.2\times10^{-4}) - 0.015. \qquad (5)$$

Here ν represents the attempt to escape frequency, which typically is between 10^{10} and 10^{12}, and E_{tp} and E_v are the hole-trap energy and SiO_2 valence band energy, respectively. Because ΔE does not strongly depend on ν, the value assumed for ν is not significant. However, it can be estimated more closely by producing spectra at two different sweep rates, β_1 and β_2, and measuring the temperature, at say T_1 and T_2, at which some prominent peaks in the spectra appear. Then ν can be determined from the expression

$$\nu = 10^{y} \qquad (6)$$

where

$$y = [(T_2 \log_{10}\beta_2 - T_1 \log_{10}\beta_1)/(T_2 - T_1)] - 1.66 \qquad (7)$$

3.3 Irradiation Conditions

All samples were irradiated either with 1-MeV electrons in a van de Graaff acccelerator or with 10.2-eV VUV photons in a VUV spectrometer. Only samples with semitransparent Al electrodes approximately 100- to 200-Å thick were exposed to VUV irradiation. This allowed a large percentage of the VUV photons to impinge upon the SiO_2 while a bias was being applied. Photons of energy greater than 8.0 eV provide a useful tool for examination of the hole-trapping phenomenon in SiO_2, since they are strongly absorbed. Powell has measured the optical absorption in unsuppported SiO_2 films grown on silicon and found a bandgap of 8.0 ± 0.2 eV and an optical absorption coefficient at 10.2 eV of 1.05×10^6 cm^{-1}.[19] Thus, for a 650-Å film only about 1% of the photons that enter the oxide reach the silicon interface. This strong absorption allows selective transport of either electrons or holes, depending upon the bias during irradiation. The experimental arrangement for VUV irradiation is shown in figure 3.

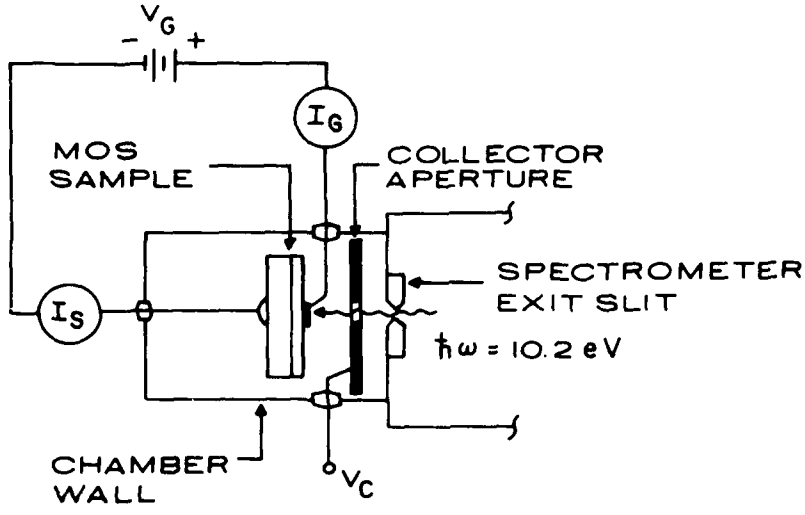

Figure 3. Experimental arrangement used for VUV irradiation.

[19] R. J. Powell and M. Morad, J. Appl. Phys. 49(4), 2499 (1978).

For data taken from samples irradiated with VUV irradiation, it is useful to relate the photon fluence to an equivalent dose from 1-MeV electron irradiation. Because the VUV irradiation is almost totally absorbed whereas 1-MeV electrons lose very little of their energy in 650 Å of SiO_2, it is meaningless to compare dose delivered to the surface in each case. These measurements would be meaningful only if the SiO_2 thickness had been much greater than the extrapolated range of 1-MeV electrons.

We are interested in comparing primarily "dose" in terms of equivalent numbers of hole-electron pairs generated. We have found that at typical photon fluences of 3×10^{11} $s^{-1}cm^{-2}$ a total dose of 10^6 rad is delivered in approximately 200 s.[16] This is equal to a dose rate of 5000 rad/s, about half of the dose rate used for 1-MeV electron irradiation but considerably larger than typical ^{60}Co dose rates of 250 rad/s.

4. PREIRRADIATION MEASUREMENTS

As discussed in section 2.3, the wafers were metallized either with 12×10^3 Å of Al for chips that were to be mounted on headers or with approximately 100-200 Å Al for wafers that were to be irradiated with VUV. These differences in metallization, it appears, were responsible for large differences in the preirradiation behavior of these oxides, even though they did not significantly influence radiation hardness.

Most of the wet-oxide wafers from pyrogenic oxide lots 06168 and 06128 contain significant levels of mobile ions, and in some cases the thin-metal wafers have a slow-trapping instability.[20] We do not believe the slow-trapping instability to be related to the mobile-ion levels in the oxide, because it occurs only in the thin-metallization wafers. The cause of the higher mobile-ion contamination in the wet-oxide wafers is not known; it should be noted, however, that it apparently does not affect the radiation hardness adversely (see table 3).

[20] E. H. Nicollian, J. Vac. Sci. Technol. 14(5), 1112 (1977).

The wafers studied in greatest depth were those that had a forming gas (FG) sinter step in the process. It has been claimed in the literature that a forming gas Al sinter actually exacerbates the slow-trapping problem.[7] We are not convinced of this; in fact we have seen it do just the opposite in samples with thin metallization. For lots 06168 and 06128, although both had an FG sinter, none of the thick-dot capacitors measured had a slow-trapping instability. There is also some evidence that organic contaminants can enhance slow-trapping instabilities.[21] Since all the samples were stored after fabrication in individual plastic boxes believed to be made of polymethyl methacrylate, the organic vapors in these boxes may very well have diffused through the thin dots, but not the thick ones. This also could have created the instabilities we have seen.

4.1 Slow-Trapping or Negative-Bias Instability

Slow-trapping or negative-bias instability is the name commonly given to the phenomenon responsible for the negative flatband or threshold voltage shift observed under negative-bias stressing of MOS oxides.[20] This is a temperature-activated phenomenon and may or may not be important at room temperature. It is called slow trapping probably because of its observed time dependence at room temperature and the fact that trapping is thought to be the only mechanism capable of explaining this observed behavior.

Figure 4(a) shows the high-frequency capacitance-voltage (CV) curves before and after negative-bias thermally stimulated current (TSC) stressing of a (thin-metal) capacitor. Figure 4(b) shows the resultant TSC emission current as a function of temperature. The curve labels refer to the sequence of CV and TSC measurements described below. The measurement sequence was as follows:

(1) Measure HFCV curve.

(2) Bias at -13 V (-2 MV/cm) and heat to 525 K while measuring the TSC characteristic.

---

[21] H. Nakayama, Y. Osada, and M. Shindo, J. Electrochem. Soc. 125(8), 1302 (1978).

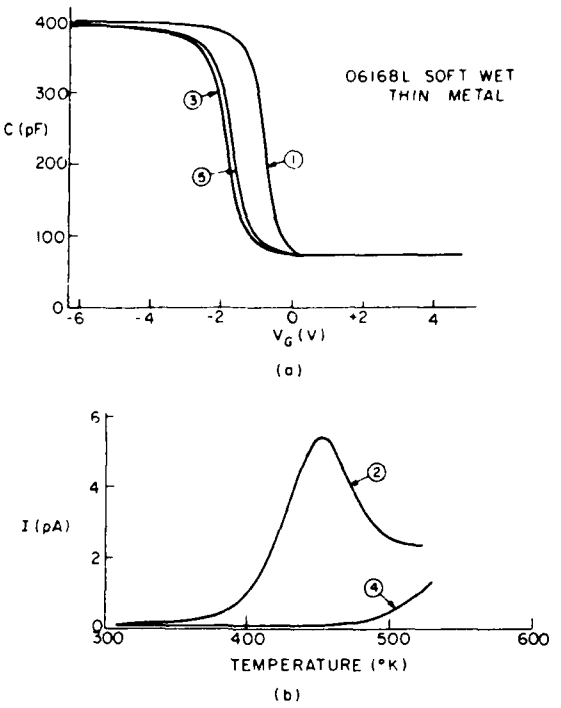

Figure 4. CV and TSC measurements. (a) HFCV curves before and after negative-bias TSC stressing. (b) Resultant TSC curves (see text).

(3) Cool down to room temperature under negative bias and measure another HFCV curve.

(4) Bias at -13 V and repeat step 2.

(5) Cool down under negative bias and measure another HFCV curve.

Ion motion is not responsible for the flatband shift observed, since it is in the wrong direction for negative bias. Conceivably, position ion motion still may be involved if it is accompanied by a large increase in interface states near the silicon conduction band as the ions are drawn away by the negative bias. However, this would assume a sizeable initial ion concentration at the Si/SiO_2 interface, and no such concentration has been observed. (Recently it was shown that mobile ions can cause a large density of interface

states near the silicon conduction band.[22] However, this was observed under positive bias stressing.) Under negative bias, hole injection and trapping might occur as a result of either direct tunneling to traps from the silicon valence band or of Fowler-Nordheim (FN) tunneling[23] through the triangular barrier from the silicon valence band with subsequent trapping. Figure 5 illustrates these two possibilities. Direct hole tunneling appears highly improbable since it would be very bias sensitive (no such sensitivity has been observed). Hole trapping by FN tunneling, on the other hand, would not have the temperature dependence that we observed. Fowler-Nordheim tunneling without trapping has a temperature dependence of the form

$$J(T) \propto \frac{\pi kT/d}{\sin \pi kT/d} \quad \text{where } kT/d < 1 \tag{8}$$

with $kT/d \simeq \frac{1}{2}$ near room temperature.[24] Thus, the current density should increase monotonically with temperature and rise rapidly near 600 K. In the presence of hole traps very close to the silicon interface, this current density would be multiplied by a factor that takes into account the decreasing probability of capture as traps are filled. This factor would be ≤ 1 and increase monotonically with temperature. The observed structure in the thermal current can therefore not be explained by FN hole tunneling with trapping.

Field emission of electrons from neutral traps appears to be the most plausible explanation for both the flatband shift and thermal current observed. Consider the process shown in figure 6. Under elevated temperatures, electrons are thermally emitted into the SiO_2 conduction band. With a high field applied these electrons are rapidly swept out of the oxide, leaving the positively charged centers behind. In order to explain our data these centers must be located throughout the oxide rather than very close to either interface. If

---

[22] M. Schulz and E. Klausmann, J. Phys. D (Appl. Phys.) 18, 169 (1979).
[23] M. Lenzlinger and E. H. Snow, J. Appl. Phys. 40, 278 (1969).
[24] Z. Weinberg, W. Johnson, and M. Lampert, J. Appl. Phys. 47(1), 248 (1976).

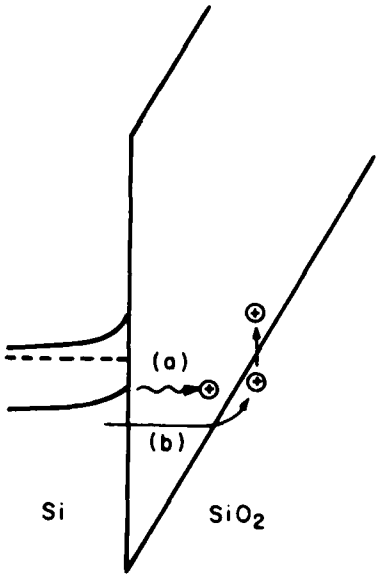

Figure 5. Proposed trapping mechanisms. (a) Direct-hole tunneling into traps from Si valence band. (b) Fowler-Nordheim tunneling followed by trapping.

they were all at the Si/SiO interface, a flatband shift would be recorded but no current would be observed. On the other hand, if they were all at the Al/SiO_2 interface, a current would be measured but no flatband shift would be recorded.

This can be shown more quantitatively by referring to figure 7. If total charge Q_o is left in the oxide having a centroid $\bar{x}$, then the flatband shift resulting from this charge is

$$\Delta V_{FB} = \frac{L - \bar{x}\, Q_o}{L\, C_{ox}} \tag{9}$$

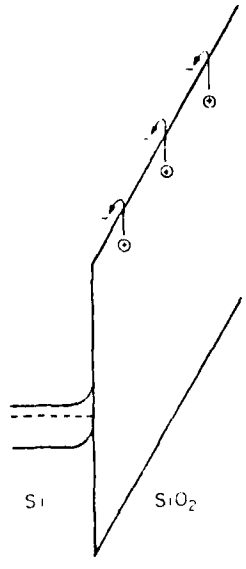

Figure 6. Temperature-assisted field emission of electrons from neutral traps near SiO_2 conduction band.

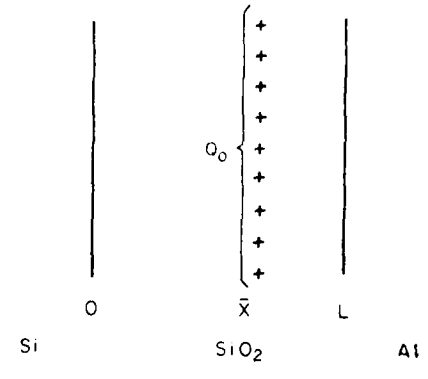

Figure 7. Schematic of charge-transport mechanism. Coordinates are referred to Si interface.

where C_{ox} is the oxide capacitance. The total charge collected by the external circuit, however, is given by

$$Q_c = \frac{\bar{x}}{L} Q_o \tag{10}$$

since on the average the charge carriers move only a distance $\bar{x}$. If we let

$$r = \frac{Q_c}{C_{ox}\Delta V_{FB}} \tag{11}$$

where r is defined as the ratio of the collected charge to the charge reflected by the flatband shift ΔV_{FB}, then it can easily be shown that

$$\bar{x} = \frac{r}{1 + r} L \tag{12}$$

For the sample shown in figure 4 this means that the electrons are emitted from the neutral traps having a centroid about 120 Å from the Al interface.

The temperature dependence we observed is quite repeatable from sample to sample and is somewhat dependent upon bias between 1 and 2 MV/cm. If electrons are thermally emitted from traps, this peak is then characteristic of the thermal trap depth. The bias-dependence effect can probably be explained by Frenkel-Poole lowering of the neutral trap short-range potential barrier.[25-27]

Some work done with negative corona discharge by Woods and Williams[28] and Weinberg et al.[24] further supports this argument. Woods and Williams found that large negative flatband shifts could be induced in $Hg/SiO_2/Si$ capacitors formed over areas of SiO_2 subjected to a negative corona discharge. They postulated either field emission of

[25] J. G. Simmons, Phys. Rev. 155, 657 (1967).
[26] P. C. Arnett and N. Klein, J. Appl. Phys. 46, 1400 (1975).
[27] A. K. Jonscher, Thin Solid Films 1, 213 (1967).
[28] N. N. Woods and R. Williams, J. Appl. Phys. 47(3), 1082 (1976).

electrons from neutral traps or FN tunneling of holes from the Si with subsequent trapping. When they found it impossible to trap photoinjected holes from the silicon substrate, they ruled out FN tunneling and the trapping of holes, concluding that field emission of electrons had to be the mechanism responsible. Weinberg et al. performed negative corona experiments on SiO_2 grown over a pn junction. With this structure the sign of the charge carrier in the SiO_2 can be determined. This group of researchers concluded that electrons were the dominant charge carriers in the SiO_2 during negative corona.

The weight of the evidence we have presented, supported by the above arguments, leads us to conclude that the slow-trapping phenomenon observed in these samples is caused by the field emission of electrons from neutral traps located approximately 120 Å from the Al/SiO_2 interface, with a peak at 450 K. Assuming an attempt-to-escape frequency of 10^{11} s^{-1}, we calculate from equation (5) an effective trap depth of 1.14 eV below the conduction band of the SiO_2.

4.2 Mobile Ions

Although evidence of the presence of mobile ions has been found in both the wet and dry oxides to different degrees, it did not detract from the radiation hardness of any of the hardened samples. In samples with thin metal the evidence usually pointed to uniform distribution across the area of the capacitor, whereas in the thick-metal capacitors the distortion had lateral non-uniformities (LNUs).

Figure 8 shows HFCV and TVS curves for a soft wet sample with a thin Al gate. The two CV curves are the initial curve and the curve measured after a ⊕ · ⊖ · ⊕ TVS sweep with the cooldown at +10 V. The TVS curve was measured at 360°C. Based on equation (1), the integrated mobile ion peak corresponds to an average ion concentration of 1.83×10^{11} cm^{-2}. This is equivalent to a -0.56 V shift in the CV curve if all ions are at the Si/SiO_2 interface. The measured shift between the CV curves in figure 8(a) is approximately equal to -0.60 V, a value in fairly good agreement with theory. Since the CV shift is nearly parallel and its magnitude in agreement with the TVS measurement we can conclude that ions are responsible and that they are uniformly

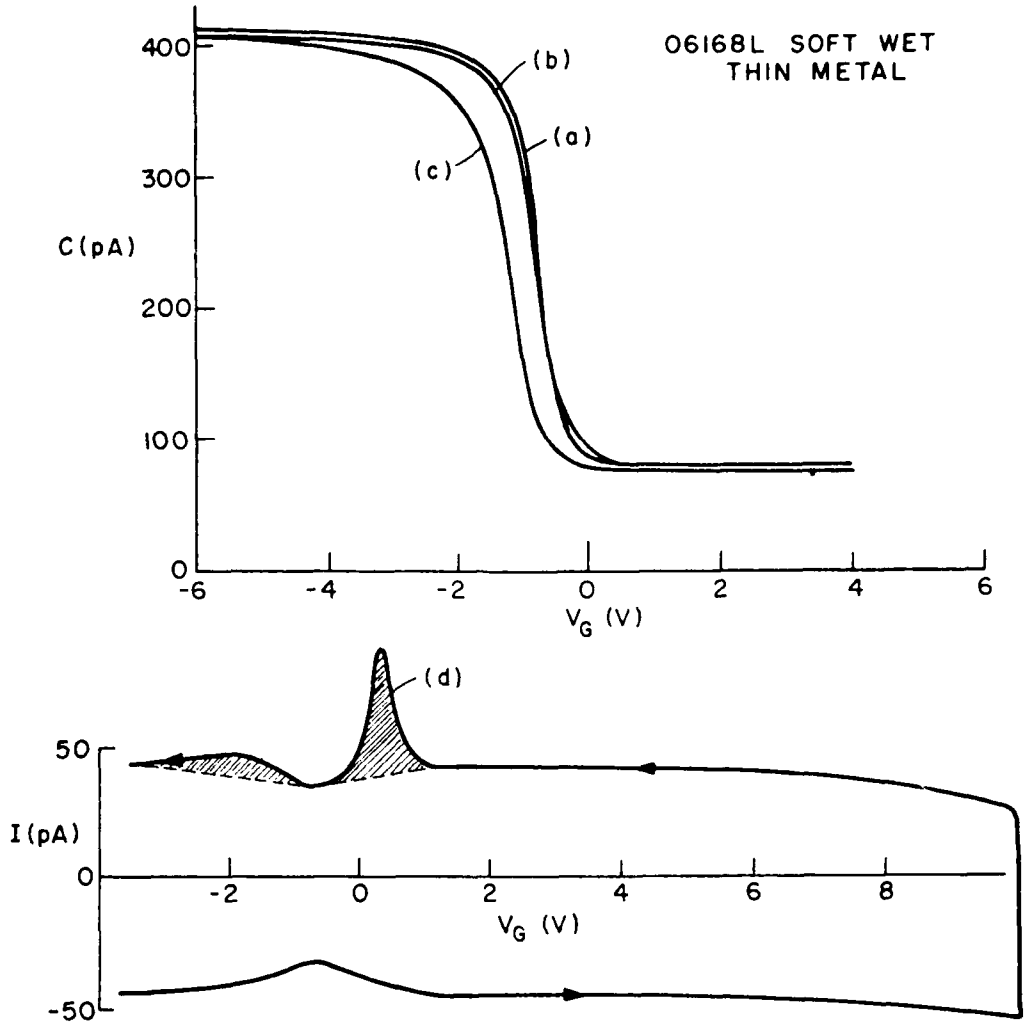

Figure 8. CV and TVS measurements on sample 06168L. (a) Initial CV curve; (b) CV curve after ⊕ → ⊖ sweep; (c) CV curve after ⊖ → ⊕ sweep; (d) TVS curve: α = 0.1 V/s, T = 300°C. Total mobile-ion concentration $N_M = 1.8 \times 10^{11}$ cm^2.

distributed across the capacitor. Following Derbenwick's arguments, we can assign the large peak at +0.2 V to sodium (Na) and the flat minor peak to potassium (K).[12]

Figure 9 shows the same measurements on a wafer from the same lot as the one shown in figure 8, but with a thick-metal-capacitor dot. Here the K peak is considerably larger than before and there is evidence of LNUs in the ion distribution. The initial and final CV curves are hardly shifted at all over most of their length except in inversion where the final CV curve has a long "tail." The integrated ion current corresponds to a CV shift of $\sim$3.2 V for a uniform distribution of ions. As this can obviously not be the case, we must conclude that if the current is due to ions that most of the ions are concentrated in a small area of the capacitor. We suspect that this area is an annular region around the edge of the MOS dot and that the ions came in contact with the sample after the metal definition step, probably

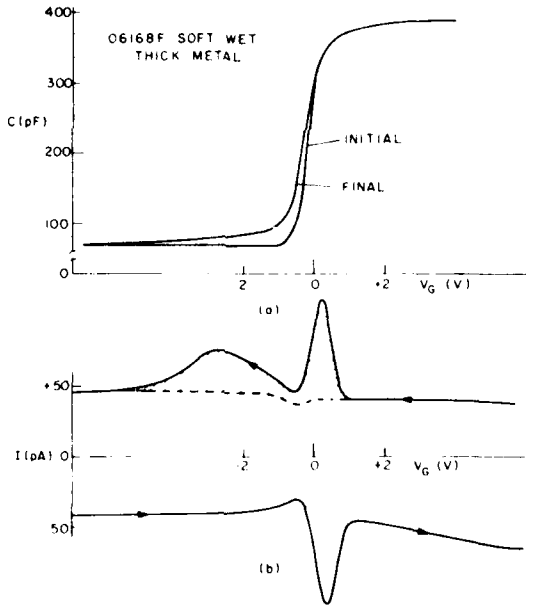

Figure 9. CV and TVS measurements (wafer no. 06168F). (a) CV curves before and after TVS measurements at 300°C. Final curve measured after cooldown at +8 V. (b) TVS curve at 300°, α = 0.1 V/s. Total mobile-ion concentration $N_M = 1.04 \times 10^{12}$ cm^{-2}.

during etching or photoresist removal. Figure 10 shows the same type of data for a hard-wet sample with thick metal gate. Another possibility is that the current measured is caused by the slow-trapping instability described in the previous section. However, this is unlikely because once these neutral traps are emptied of electrons, a changing bias should not change their occupancy. In addition, the TSC measurements described in section 4.1 indicate that the electrons should be emptied during the heat-up phase of the TVS measurement.

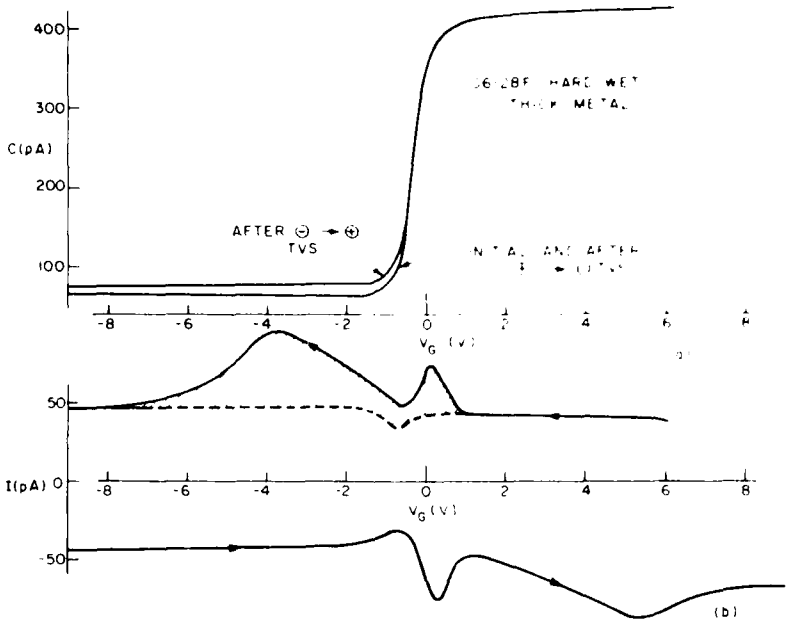

Figure 10. CV and TVS measurements (wafer no. 06128F). (a) CV curves before and after TVS measurements at 300°C. (b) TVS curves at 300°C, α = 0.1 V/s. Total mobile-ion concentration $N_M = 1.53 \times 10^{12}$ cm^{-2}.

Figure 11 shows CV and TVS data for a hard-wet thin-metal capacitor. The CV plot is on an expanded scale to show the small shifts more closely. The first TVS curve, starting from +13 V, shows a small Na mobile ion density of 3.5×10^{10} cm^{-2}; this would correspond to a 0.11-V CV shift (b). After cooling down at +13 V and measuring the CV curve (c), a second TVS plot was made, starting from -13 V (d) and finally

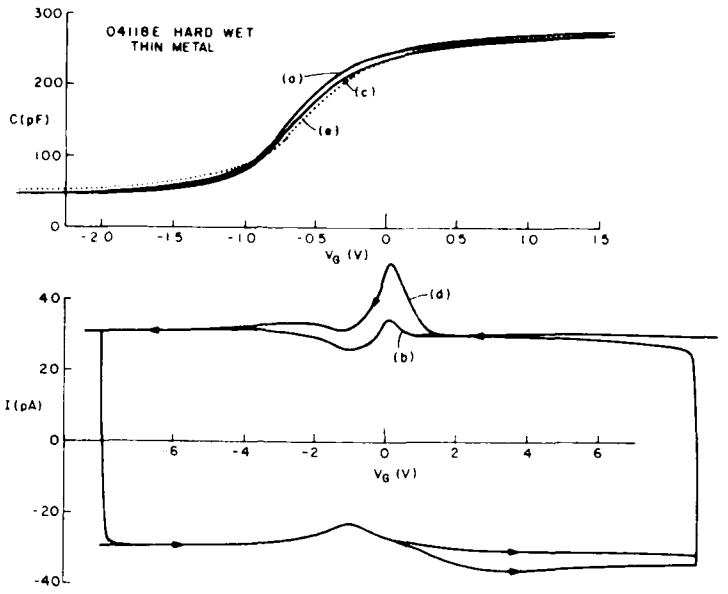

Figure 11. CV curves and TVS curves for wafer no. 04118E. (a) Initial CV curve; (b) first TVS curve starting from +13 V; (c) CV curve after first TVS with cooldown at +13 V. (d) Second TVS plot, starting and finishing at -13 V; (e) CV plot after second TVS plot; TVS measured at 300°C with α = 0.1 V/s. Total initial mobile-ion concentration $N_M = 3.5 \times 10^{10}$ cm^{-2}.

ending and cooling down at +13 V. The final CV trace is (e). From curve (d) the apparent ion density is 1.46×10^{11} cm^{-2}, corresponding to a CV shift of 0.45 V. A comparison of the initial CV curve (a) and the final curve (e) shows a shift no greater than 0.15 V over most of their lengths, except in inversions. The apparent LNU ion charge and increase in ion density together suggest that ions were pulled in from the edge of the capacitor during the bias-temperature stressing of the TVS measurements. This observation is important since it raises doubts about the ability of TVS measurements to measure radiation-enhanced mobile ions, as Repace has claimed it can.[29,30] This will be discussed further in section 5.

[29] J. Repace, IEEE Trans. Nucl. Sci. NS-24(6), 2088 (1977).
[30] J. Repace, IEEE Trans. ED-25(4), 492 (1978).

Figure 12 shows results of TSC measurements on a sample containing mobile ions. TSC stressing under positive bias was done first, followed by negative TSC stressing. The CV curves show that the instability in this particular sample can be classified as mobile ions. Several features of the TSC spectra are worth noting. Under positive TSC a slight peak occurs at 450 K, the same temperature at which occurred the slow-trapping phenomenon described in section 4.1. Under negative TSC stressing, peaks occur at 335 and 530 K. Because of the behavior of the CV shift, we must assign these to mobile ions. The temperatures at which these peaks occur are the same as those measured

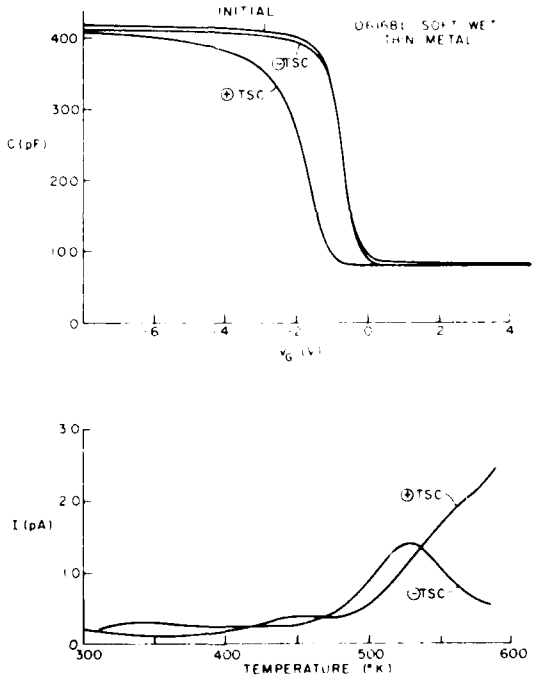

Figure 12. CV and TSC measurements on soft wet sample no. 06168L having mobile ions. Positive TSC stressing at +5.5 V was followed by CV measurement, negative TSC stressing at -8.7 V, and the final CV curve as shown. β = 0.2 K/s.

by Nauta and Hillen[31] in deliberately contaminated samples and lead us to believe that the peak at 335 K is sodium and that at 530 K is potassium.

The complete recovery of the CV shift under negative TSC stressing raises questions about assigning slow trapping to the 450 K peak (see section 4.1). These traps might be tied up in some fashion with the ions in the lattice, and moving the ions around might change the occupancy and charge state of the slow traps. A reversal in the order of the TSC stressing gives results that support this hypothesis. Figure 13 shows these data. An initial negative TSC stress yields the

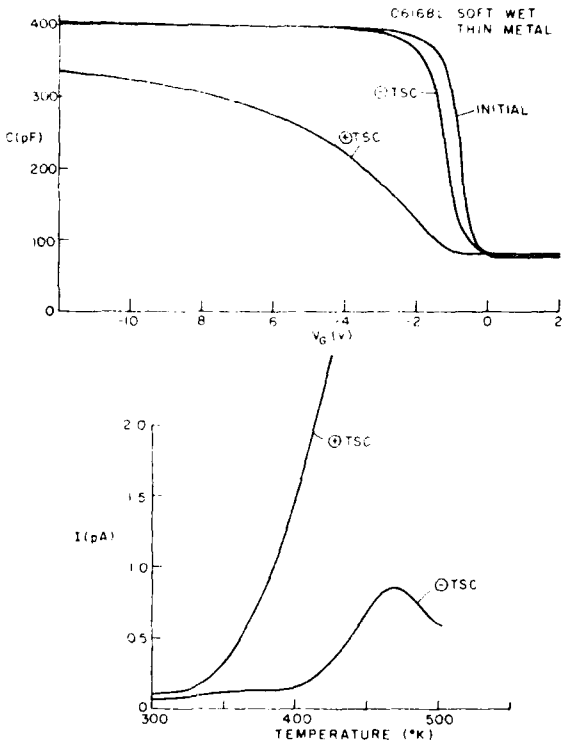

Figure 13. CV and TSC measurements on sample from same wafer as shown in figure 12. Negative TSC stressing at -7.5 V was followed by CV measurement and then positive TSC stresssing at +5.1 V. β = 0.2 K/s.

[31] P. Nauta and M. Hillen, J. Appl. Phys. 49(5), 2962 (1978).

characteristic peak at 450 K and the negative CV shift that indicates slow traps. A subsequent positive TSC stress shows a grossly distorted and negatively shifted CV curve indicative of mobile ions. The monotonic increase in the TSC current may be due to local high-density ion clusters creating fields large enough to enhance tunneling.

These mobile-ion measurements show that conventional CV bias-stress testing can make LNU ion densities appear to be small, although in fact, as the TVS measurements prove, they are in some cases quite large. In addition, the radiation data in table 3 show that the apparent high ion densities do not compromise the hardness of the hardened oxides. On the other hand, there does appear to be some interaction between mobile ions and trapped holes, which seems to be limited to affecting the thermal annealing characteristics of these oxides (see section 5).

5. POSTIRRADIATION BEHAVIOR

Both the hard wet and hard dry oxides show similar levels of radiation hardness, although the thermal annealing characteristics of the hole traps in wet and dry oxides are quite different. This appears to be mainly due to the presence of a high density of mobile ions and a slow-trapping instability in the wet oxide samples.

5.1 Dry Oxides

The TSC measurements on irradiated dry oxides are more consistent than the wet-oxide measurements, but they are also the least interesting in terms of the information they provide. Figure 14 shows the CV curves and postirradiation TSC curve for a hardened-dry-oxide capacitor mounted on a header. This particular sample was irradiated with 1-MeV electrons to 10^6 rad under +10 V bias. After irradiation the bias was held on the sample for 30 min before the negative-bias TSC measurement was begun. This was not essential, as all samples exhibited the same TSC response whether they were biased for 30 min or 1 min after irradiation. The figure shows that the TSC spectrum has no noticeable structure except near 600 K, where a large increase takes

place. The area under the curve represents 6.4×10^{11} charges cm^{-2} or an equivalent ΔV_{FB} of 1.96 V, referred to the silicon interface. This is about twice as large as the ΔV_{FB} measured from the CV curves, and probably is in error because of Fowler-Nordheim tunneling current at higher temperatures. The failure of the CV curve to revert to its preirradiation position up to 600 K indicates that most of the holes are trapped quite deep (>1.6 eV above the valence band). The same type of behavior was seen for soft dry oxides.

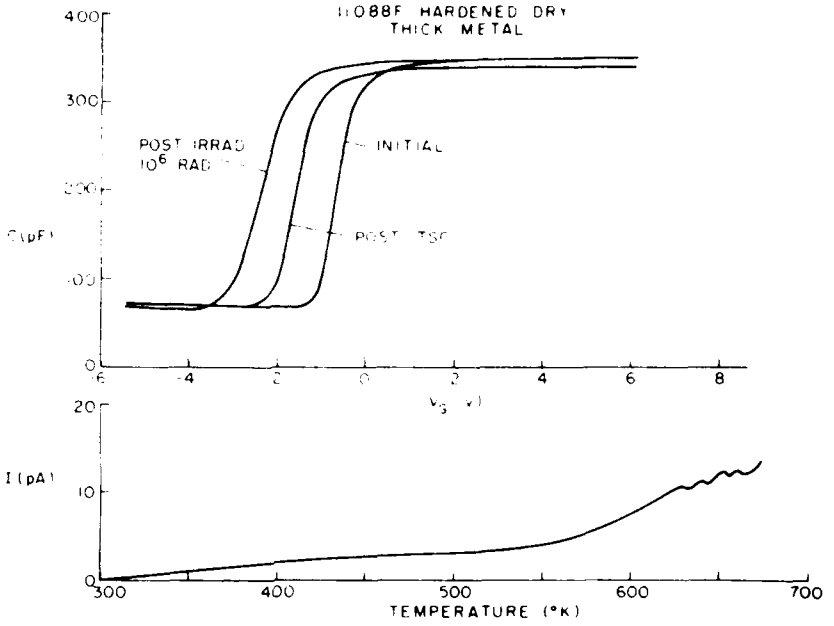

Figure 14. CV and TSC measurements on hardened-dry-oxide capacitor no. 11088F. $\beta = 0.2$ K/s; $V_G = -13$ V.

5.2 Hard Wet Oxides

Most hard wet oxides did not have any distinctive structure under initial negative TSC stress, even though TVS measurements gave evidence of the presence of a high density of mobile ions (see fig. 10). This indicates that all i ns are close to the Al interface after growth. Figure 15 illustrates he behavior representative of most of the hard wet oxides examined. 'his particular sample had a thin-metal gate and was irradiated under +(.5 V with VUV photons for 400 s, a dose

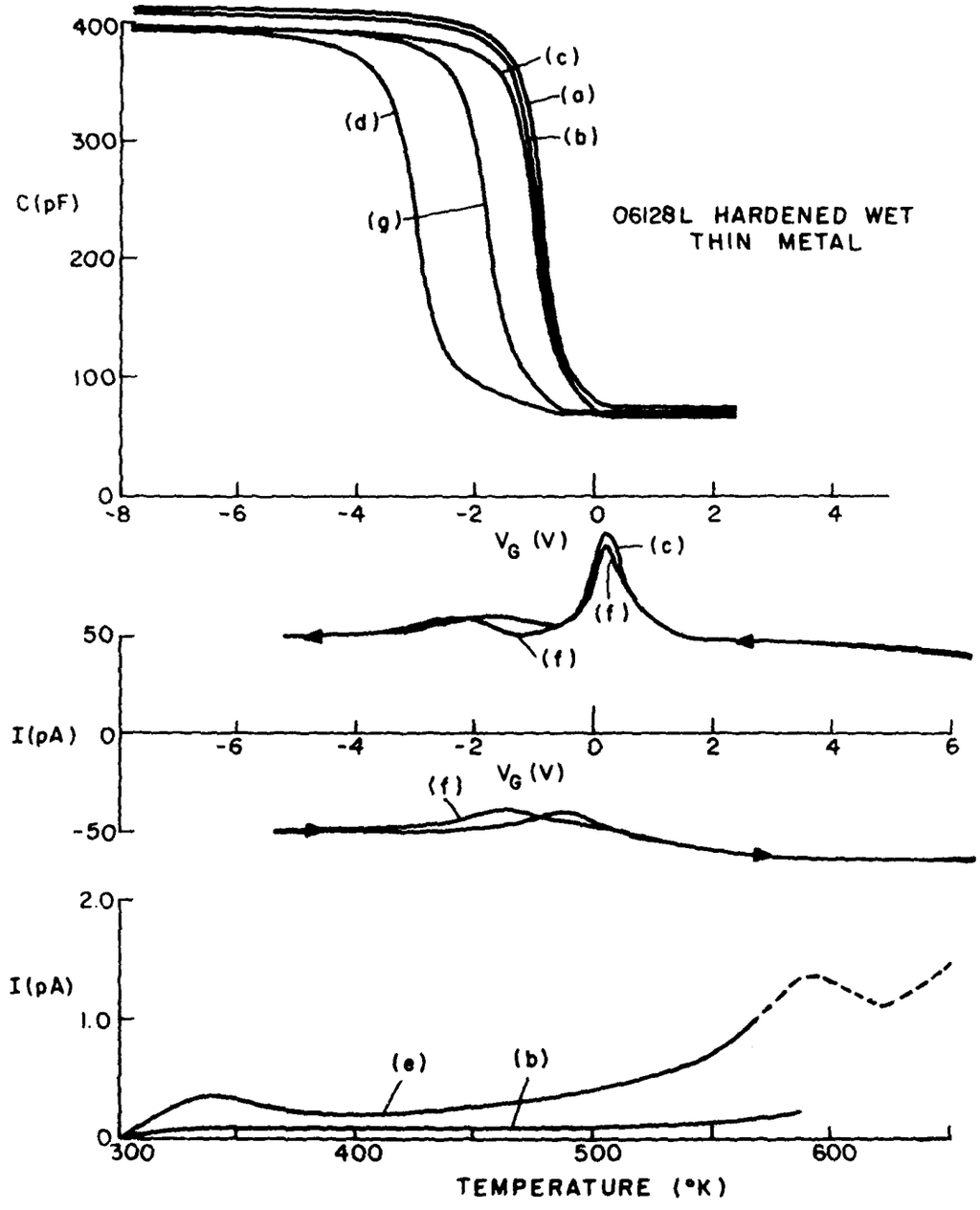

Figure 15. CV, TVS, and TSC measurements on hardened wet sample no. 06128L (for sequence of measurements see text). Irradiation was VUV for 400 s. During TSC, $\beta = 0.2$ K/s. Total mobile-ion concentration $N_M = 2.78 \times 10^{11}$ cm^{-2}.

roughly equivalent to a 2-Mrad dose in terms of the number of hole-electron pairs generated. The following sequence of measurements is important in understanding the results shown in figure 15:

(a) The initial CV curve was measured.

(b) The initial TSC curve was measured at a bias of -13 V with a temperature sweep of 0.2 K/s. After cooldown at bias another CV curve was plotted.

(c) After heating at a bias of -13 V to 573 K (300°C), a TVS measurement was made sweeping at 0.1 V/s from -13 to +7 V and back to -13 V again. After cooldown at -13 V another CV curve was plotted.

(d) The sample was irradiated at +6.5 V for 400 s and allowed to relax at bias for another 400 s. Another CV curve was plotted.

(e) A second TSC measurement was made at -13 V bias.

(f) Without cooling down a TVS measurement was made, starting at -13 V, sweeping to +7 V, and then back to -13 V.

(g) After cooldown at -13 V a final CV measurement was made.

The initial TSC measurement and CV curve (b) show that the density of mobile ions at the Si interface was negligible and that no slow trapping occurred. However, the first TVS measurement discloses a net mobile ion density of 2.78×10^{11} cm^{-7}, indicating pile-up at the Al interface.

Irradiation and subsequent negative TSC annealing produced two peaks in the TSC spectrum, one at 335 K and one at 585 K [the dashed portion of TSC curve (e) was not actually measured on this sample, but it did appear on others from the same wafer]. These are the peaks that we have previously assigned to Na and K. At this point it might be assumed that the irradiation actually liberated Na and K from previously uncharged states.[29] However, the second TVS curve (f) shows that within experimental error the actual mobile-ion density did not increase. In addition, the integrated TSC current yields a collected

charge of 3.78×10^{11} charges cm^{-2} for the whole sweep, corresponding to a CV flatband shift of 1.16 V. The actual measured flatband CV shift between CV curves (d) and (g) is 1.2 V. This indicates that all of the collected charge is at the Si interface. We interpret all this to mean that the peaks on the postirradiation TSC curve (e) are associated with movement of ionic charge from the Al interface to the Si interface during irradiation and subsequent movement back under negative TSC. No new ionic charge is created. Thus, it is possible that these oxides would be harder if the mobile ions were absent.

TVS measurements on irradiated soft wet samples also reveal similar information about the nature of the trapped holes. Figure 16 shows TVS curves for a soft wet-oxide capacitor. This was a thick-metal device mounted on a header. The device was irradiated to 10^6 rad with 1-MeV electrons, resulting in a ΔV_{FB} of approximately 35 V. TVS measurements were made after irradiation by first heating under a bias of +7 V to 573 K (300°C) until the measured current decayed to <5 pA. The TVS sweep was then started, going from positive to negative bias, and then back again to positive, at a sweep rate of 0.1 V/s. The curves labeled 1, 2, and 3 refer to the 1st, 2nd, and 3rd sweeps, respectively. It is evident from these data that charge is being removed from the oxide each time the TVS sweep is cycled. We believe these charges to be trapped holes that were not detrapped during the positive-bias heat-up period. Simple Frenkel-Poole emission from traps with field-assisted barrier lowering obviously does not explain these data.[25,26] The barrier would be at its lowest point at the extremes of the voltage sweep, not during the middle of the sweep where most of the charge motion is taking place. The most plausible explanation is that the trapped holes are in traps associated with the mobile ions, and that movement of these ions puts the holes into a more energetically favorable position to be emitted. This also explains the TSC "ion peaks" seen after irradiation, as shown in figure 15. The peaks are probably not only ions but rather clusters of holes and ions that move together as the temperature is increased.

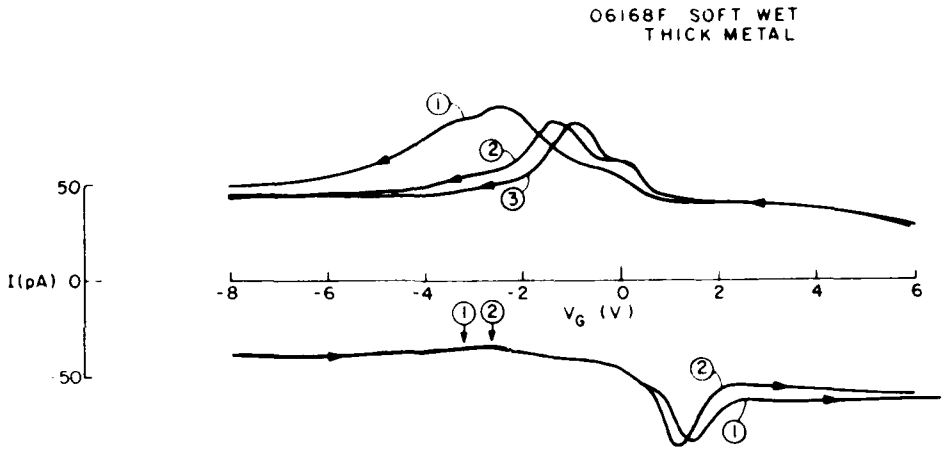

Figure 16. TVS measurements on a soft wet capacitor irradiated to 10^6 rad. Postirradiation flatband shift was about 35 V. α = 0.1 V/s.

Most of the TSC spectra for other hard wet-oxide samples resemble the spectrum shown in figure 15, except that the thick-metal capacitors that were all irradiated with 1-MeV electrons do not have very pronounced peaks at 335 K. This may be due to the different levels of Na in the thick- and thin-metal capacitors.

5.3 Soft Wet Oxides

The soft wet oxides we examined showed two different types of thermal annealing behavior, depending on whether they were thick- or thin-metal MOS capacitors.

Preirradiation negative TSC measurements on thick-metal capacitors showed no structure and only a negligible current and flat-band shift after stressing to 600 K at -13 V. Typical postirradiation behavior is shown in figure 17 for 1-MeV electron irradiation. In this figure the capacitor was irradiated to 5000 rad at +10 V bias. Bias was held for about 1 min before the sample was placed in the TSC annealing apparatus and held under a -13 V bias. The resultant TSC curve is shown in the figure. The characteristic peak at 585 K is present, but there is no apparent structure at 335 K. Based on the arguments

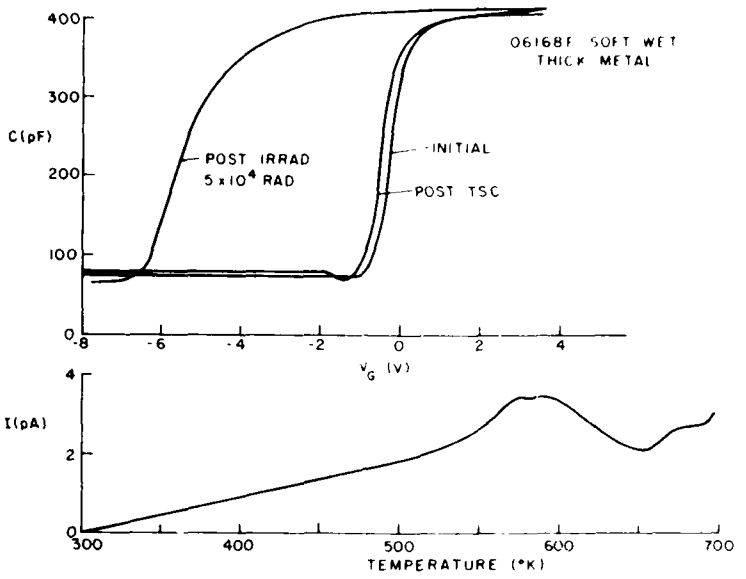

Figure 17. CV and TSC measurements on a soft wet oxide after irradiating to 5×10^4 rad. Bias during TSC was -13 V. $\beta = 0.2$ K/s.

developed above, the very large peak at 590 K and the lack of any at 335 K would appear to indicate that there was very little Na and a large amount of K in the oxide. With some of the thin-metal capacitors that showed signs of slow trapping, the postirradiation annealing conditions were dramatically different.

Figure 18 shows CV and TSC data from a thin-metal p-type capacitor. This device was irradiated with VUV without any prior TSC stressing under a +13 V bias for 16 s. The TSC spectrum under a -13 V bias was then measured. Three peaks are evident: one at 410 K, one at 450 K, and a small one at 525 K. If a preirradiation TSC curve from another capacitor from the same wafer is subtracted from that in figure 18, a large peak at 410 K and a minor peak at about 535 K remain. In addition, the difference in the collected charge from the two TSC measurements is 3.14×10^{12} cm^{-2}. This is equivalent to a 9.63-V flatband shift, exactly equal to the measured shift in figure 18. Evidently nearly all the holes are emitted during the 410 K peak, and the CV

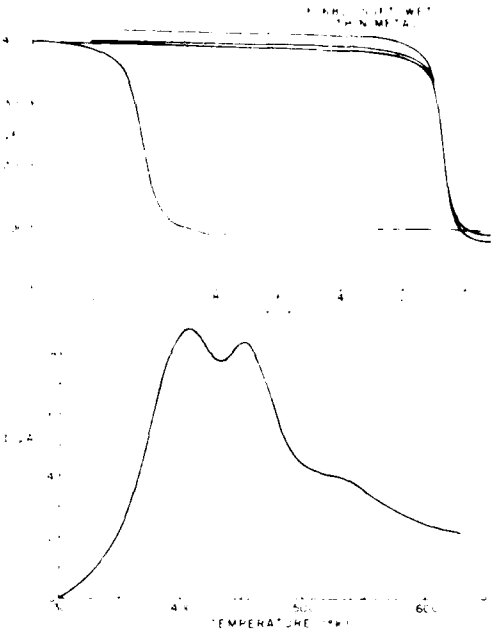

Figure 18. CV and TSC measurements on a soft wet thin-metal oxide. Capacitor was exposed to VUV for 16 s. During TSC measurement, β = 0.2 K/s; V_G = -13 V.

curve reverts back completely to the original by the end of the sweep at 623 K.

If the capacitor is subjected to a negative TSC stress prior to irradiation, the postirradiation annealing is completely different. This is illustrated in figure 19. First, the CV curve and TSC characteristics were measured. The bias during TSC measurement was -13 V. Next, the capacitor was irradiated with VUV photons for 16 s under a +13 V bias. (Note that although the flatband shift is greater in this figure than for the sample in figure 18, VUV intensity is greater as well. The ratio of flatband shifts is almost equal to the ratio of the two photon doses in each case.) After relaxation under a +13 V bias, the TSC characteristic was again measured under a -13 V bias. The sample was cooled down and the CV characteristics were measured again.

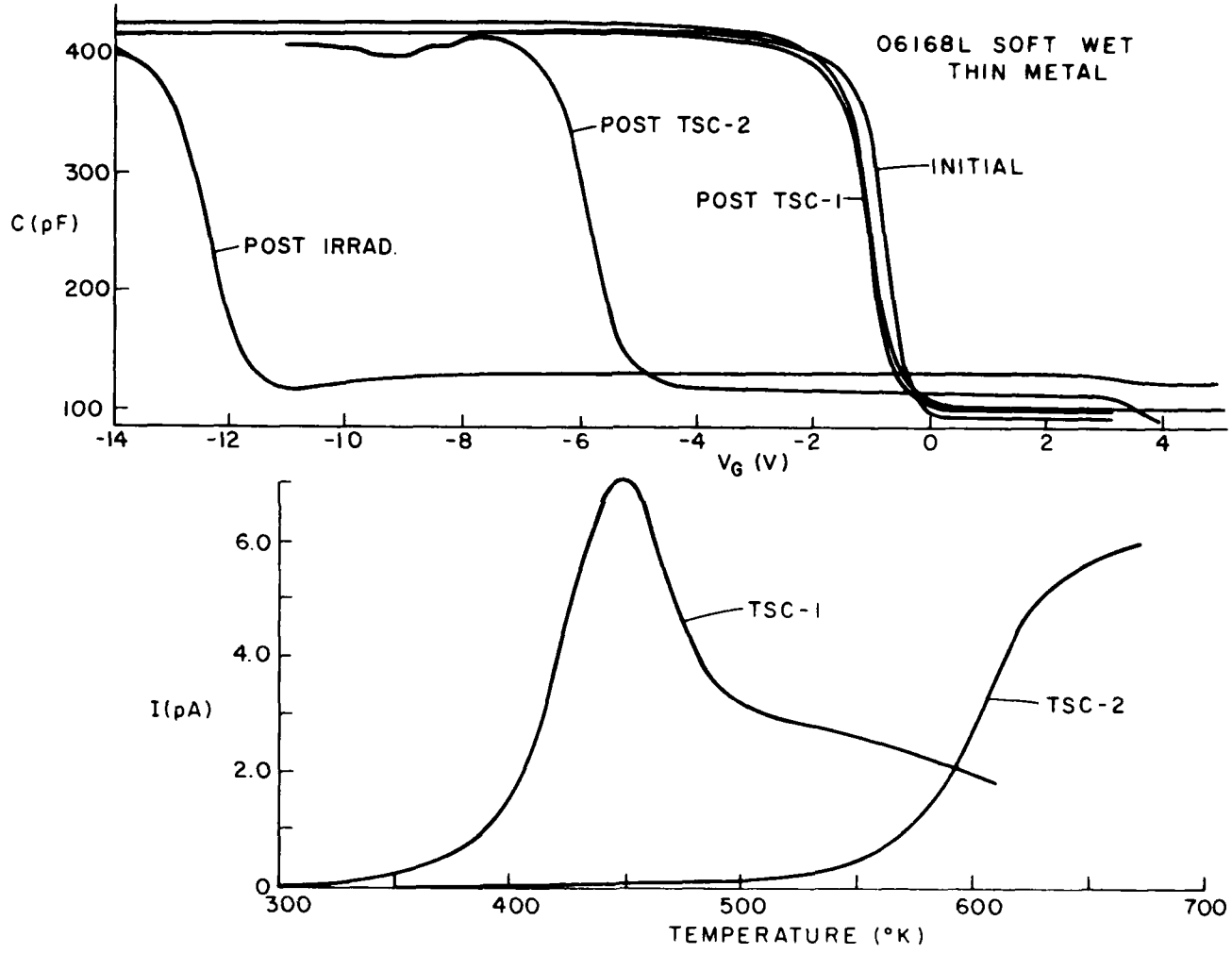

Figure 19. Preirradiation TSC measurement on capacitor from same wafer as shown in figure 18. β = 0.2 K/s; V_G = -13 V.

Note that the preirradiation thermal stressing has caused a remarkable change to take place. The trapped holes have a much higher thermal activation energy than had those in the sample that was not negative-bias temperature (BT) stressed. Both the CV shift and the emission current show that most of the holes are still trapped at 623 K. This same behavior was observed in several other samples from the same and other n-type wafers.

For small photon doses the flatband shift is linear with time and directly proportional to the product of hole trap density N_T and capture cross section σ_p.[16] From the experiment we know that the product $N_T\sigma_p$ is nearly the same for the two areas, even though the thermal emission characteristics are different. Thus, the hole-capture during irradiation is probably determined by an intermediate state which is not affected by the "slow trapping" field-emission centers. The final state of the trapped hole is, however, strongly dependent upon the occupancy of these field-emission centers as the data in figures 18 and 19 show.

6. ANALYTICAL MEASUREMENTS

For a complete characterization of the mechanism of radiation damage in SiO_2, the hole traps and interface state will have to be identified at the Si/SiO_2 interface with some chemical structure or species. Considering the density of the charges we are concerned with one might well argue that this is an impossible task at this time. For hardened oxides the density of trapped holes is on the order of $2\text{-}4\times10^{11}$ cm^{-2}. Even when it is assumed that all of these are located in a 100-Å-thick region near the Si interface, this is equivalent to a volume density of only $2\text{-}4\times10^{17}$ cm^{-3}. SIMS is capable of measuring these low levels for some elements. Ion-scattering spectroscopy (ISS) and x-ray photoelectron spectroscopy (XPS), given their current limitations, would be unable to detect such low concentrations. The situation is not hopeless, however. If we examine soft oxides we can raise the trapped-hole concentration by at least one order of magnitude. Also, since we measure electrically only those states that are charged,

there is a good chance that the actual density of states, or "disorder" at the interface, is much higher. The XPS measurements have in fact shown that there are differences between the soft and hardened oxides in terms of the intermediate-state density of Si that are well within the detectability limits of the instruments.

6.1 Impurity Depth Profiles by Secondary-Ion Mass Spectrometry (SIMS)

The technique of secondary-ion mass spectrometry is very useful for analyzing impurities profiles in solid-state materials. In its simplest form SIMS uses an ion beam to sputter a crater in the sample material and then to mass-analyze the secondary ions emitted off the material. If the sputter rate is known, the relative elemental concentration as a function of depth can be measured. The use of a known standard for the element under investigation allows absolute calibration of the intensity profile. RCA Laboratories is fortunate to have in-house a custom-built scanning SIMS instrument with a high level of sophistication.[32] This instrument possesses high sensitivity, good depth resolution, good mass spectral purity, high abundance sensitivity, and a high sputter rate. In addition to all of these characteristics, which make it superior to commercial machines currently available, it also has a scanning and secondary-ion imaging capability that permits one to observe elemental maps of the sample surface in real time as the sputtering progresses.

Of all the elements in the periodic table, hydrogen (H) and sodium (Na) are the two cited most often as being responsible for undesirable behavior in MOS devices.[5,33] We have therefore limited our SIMS analysis of the wet and dry oxides to these two elements.

Measuring H and Na profiles in SiO_2 on Si is not an easy task. Insulating films tend to charge up during ion sputtering, and this results in erroneous data. For Na the situation is even more

---

[32] C. W. Magee, W. L. Harrington, and R. E. Honig, Rev. Sci. Instrum. 49(4), 477 (1978).

[33] A. G. Revesz, J. Electrochem. Soc. 126(1), 122 (1979).

complicated in that the ion charging of SiO_2 can actually move the Na through the film and leave it piled up at the SiO_2/Si interface. Magee has solved these problems in his instrument by employing electron-beam charge-neutralization techniques and has shown the instrument capable of accurately measuring profiles of ion-implanted Na in SiO_2.[34]

6.1.1 Hydrogen Profiles

Hydrogen has been cited as being responsible for slow-trapping instabilities, irradiation behavior, dielectric breakdown, and electron trapping in SiO_2. Revesz has been the most active supporter of the hydrogen-as-contaminant school of thought.[33] He cites infrared measurements that show hydrogen atoms in thermal SiO_2 at levels of 10^{20}-10^{21} cm^{-3} (depending on processing conditions) and radiotracer analysis measurements that show 8×10^{19} cm^{-3} hydrogen atoms in steam-grown SiO_2.

We have measured hydrogen profiles in wet and dry SiO_2 as well as in a hydrogen-implanted standard. The lower limit of detection of hydrogen in insulating films is limited by the electron-stimulated desorption of hydrogen from the sample and system by the electron charge-neutralization gun. The hydrogen-desorption background level depends on the conditions prevailing in the chamber for a particular sample run; in general it scales inversely with the SiO_2 thickness being measured. Figure 20 shows a measured hydrogen profile for our hydrogen standard. This was a 7200-Å SiO_2 film grown at 1100°C in 100% pyrogenic steam. The film was then implanted with hydrogen having a peak intensity of 10^{21} cm^{-3}. In SIMS analysis of SiO_2 on Si the ^{30}Si signal is larger in the SiO_2 than in the Si due to the oxygen-enhanced yield of Si in SiO_2. This provides an easy signal for detecting the interface since the ^{30}Si signal drops significantly when the interface is reached. The measured profile shows the implanted hydrogen peak immersed in a background level of hydrogen. Scaling the intensities to the H-implant peak (10^{21} cm^{-3}) we see that the flat background located between the implant and Si/SiO_2 interface has a density of

[34] C. W. Magee and W. L. Harrington, Appl. Phys. Lett. 33(2), 193 (1978).

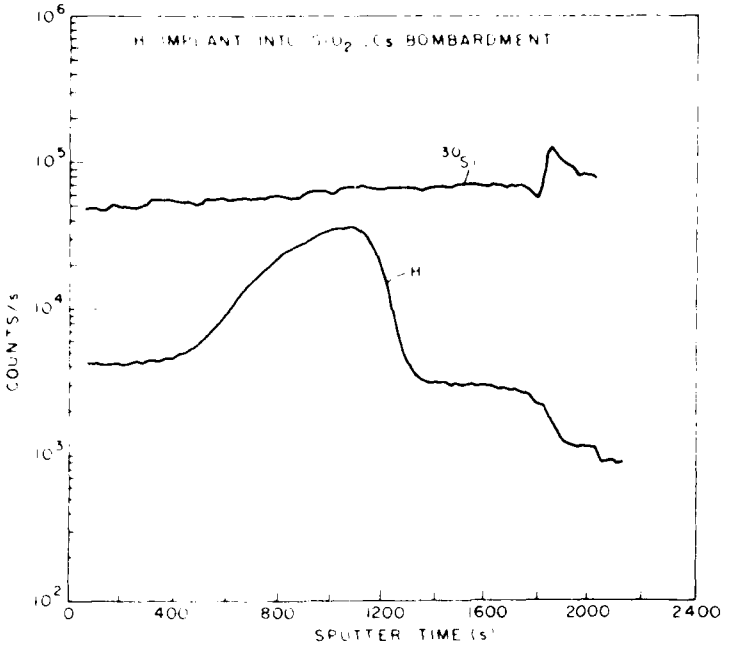

Figure 20. Hydrogen profile in hydrogen-implanted sample as measured by SIMS. Cesium was the primary ion beam. The SiO_2 film was 7200-Å thick and was grown at 1100°C in 100% pyrogenic steam.

8.5×10^{19} cm^{-3}. This is almost exactly the level measured in steam oxides with radiotracer analysis.[33] This background is real and not an artifact of the measurement technique. The fall-off in the H signal near the end of the profile is an artifact of the measurement technique and is caused by the changing efficiency of the neutralizing beam due to the proximity of the metallic silicon interface. As we stated above, the absolute lower detection limit is determined by the electron-stimulated desorption of hydrogen from sample and chamber. This can be measured by turning off the ion beam, as was done at point (a) in figure 20 (notice the abrupt drop in the Si signal), showing a hydrogen level of 2.6×10^{19} cm^{-3} for the particular operating conditions used to profile this sample.

Using the hydrogen-implanted sample, we attempted to profile hydrogen in a hard and a soft wet sample (04118C and 03068C) and a

hard and a soft dry sample (05258D and 05268D) (see fig. 21). Because these samples were only 650- to 700-Å thick, the charge-neutralization and sputter-rate conditions were different from those used for the standard in figure 20. The primary ion beam was argon rather than the cesium used before, but this did not affect the sensitivity at all. To calibrate the data the standard is profiled under the same conditions as the unknowns in a region where the absolute hydrogen level is known. Figure 21 shows these data for the standard. The region being sputtered is the sloping background near the outer interface shown in figure 20. We would expect the intensity measured in figure 21 to correspond to a hydrogen concentration of 1.15×10^{20} cm^{-3}. Figure 22 shows intensity profiles for the hard dry sample under these same conditions. Notice the drop-off in the ^{28}Si signal at 300 s. This is the Si/SiO_2 interface. However, when the ion beam is turned off at 365 s, the hydrogen signal does not drop at all. This indicates that the

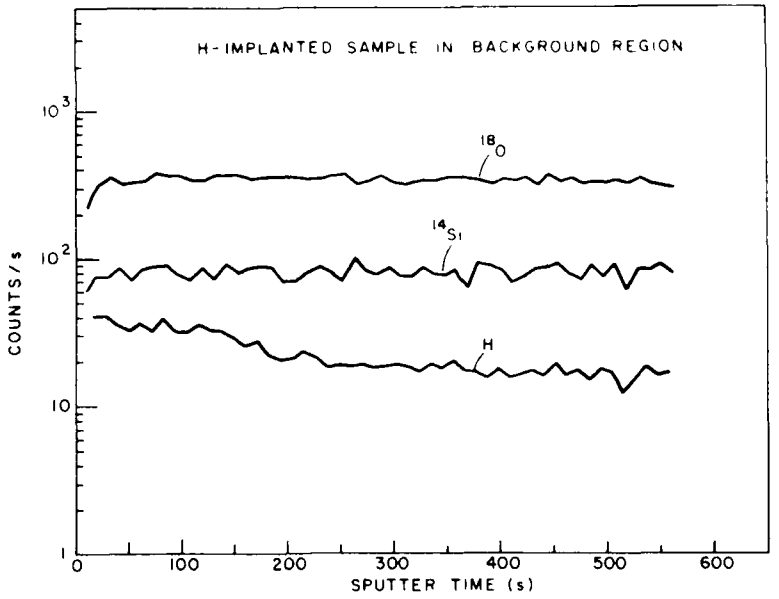

Figure 21. Hydrogen-implanted sample profile in same outer background region as shown in figure 20. The primary ion beam was argon.

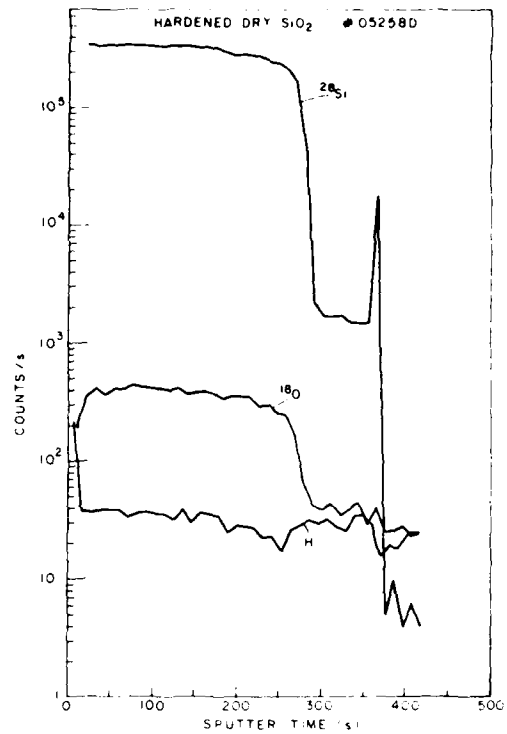

Figure 22. Profile of hydrogen, oxygen, and silicon in hardened dry oxide, sample no. 05258D. The primary ion beam was argon.

level of hydrogen being measured is the background level. Since the intensity level is the same as in figure 21, this means that for these particular operating conditions the background level of hydrogen and therefore the threshold for detection is greater than 1.15×10^{20} cm^{-3}.

It is clear from the above experiments that we cannot expect to measure hydrogen below levels of 10^{20} cm^{-3} in 700-Å SiO_2 films. However, with a film 7000-Å thick the detection limit drops to 2.6×10^{19} cm^{-3}, well below the as-grown hydrogen concentration in the steam oxide shown in figure 20.

In conclusion, these experiments tell us nothing about the hydrogen concentration in the wet and dry 700-Å SiO_2 films grown for this study. However, the measurement on the 7200-Å H-implanted steam oxide shows that the as-grown concentration of hydrogen in this oxide

is 8.5×10^{19} cm^{-3}, or about 0.2% atomic. This supports Revesz's contention that hydrogen is one of the most abundant contaminants in SiO_2. Whether it is the most important one remains to be seen.

6.1.2 Sodium and Potassium Profiles

Normally, trying to measure mobile ions like Na and K by means of SIMS is an exercise in futility because the ion-beam charging of the oxide drifts the mobile ions to the Si/SiO_2 interface. Magee and Harrington[34] were able to solve this problem with the RCA SIMS machine by employing a focused neutralizing electron beam during the argon sputtering. The results show that this technique is quite successful and makes it possible to profile implanted Na that fits the theoretical profile quite nicely.

We have profiled Na and K in one of our hard wet oxides as an independent check on the TVS electrical ion measurements. Figure 23 shows the profile of a sodium-implant standard that was used to calibrate the unknown samples measured in the same run. As the figure shows, the sensitivity of this technique is quite good, as it permits us to measure levels as low as 10^{16} cm^{-3}. The noise at the lower tail of the implant is caused by the slow count rate at these levels and thus is statistical rather than background noise. If the primary ion beam is turned off, the count drops to less than one count every 10 s, at least an order of magnitude below the lowest levels shown in figure 23. Figure 24 shows the Na and K profiles on sample 06128I in an area covered by a thin Al dot, and figure 25 is the profile on the same wafer in between dots in a bare oxide region. In both cases the Na and K are peaked at the outer interface. This may be partly due to the mutual repulsion of the ions at the high processing temperatures.[35] However, a surface layer of Na is seen on virtually all samples profiled by SIMS. Again, as we noted above, the noise in the low-level signal is statistical in nature and not background noise. Therefore, if we integrate this signal to get the total concentration per square

[35] W. Marciniak and H. M. Przewlocki, Phys. Status Solidi A 24, 359 (1974).

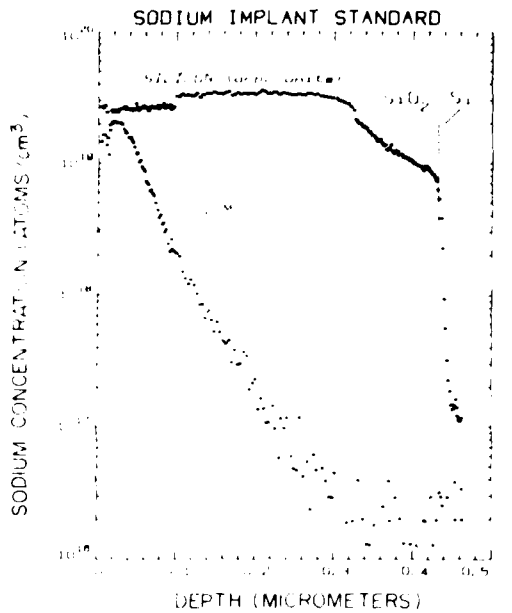

Figure 23. SIMS profile of sodium-implant standard.

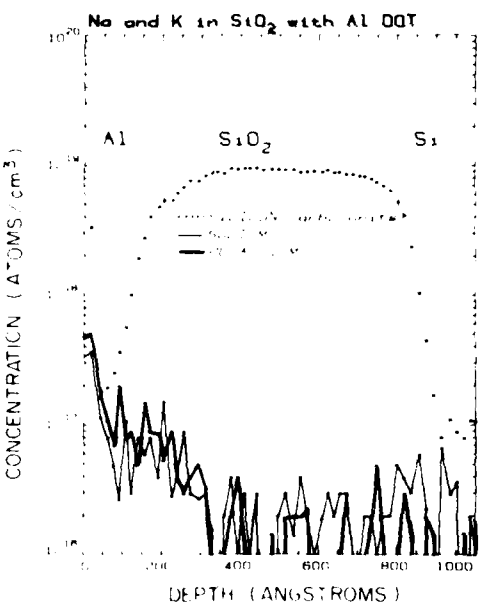

Figure 24. SIMS profile of sodium and potassium in sample no. 06128I under thin aluminum dot.

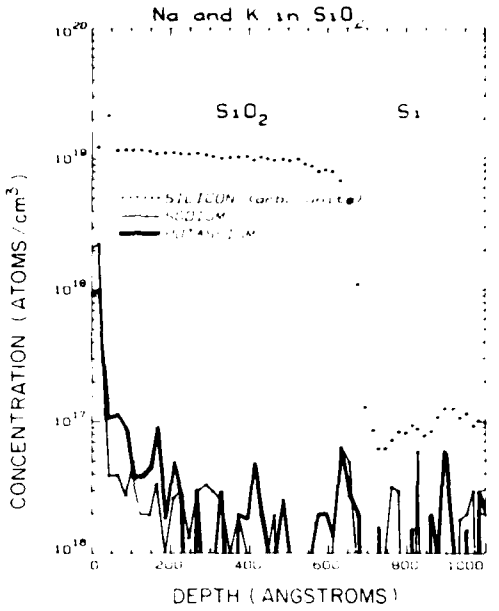

Figure 25. SIMS profile of sodium and potassium in sample no. 06128I outside of aluminum dot.

centimeter, the accuracy should be quite good. Table 4 lists these measurements for both profiles with and without the first count or interface peak being included. The K profile was not integrated, but one can see from the figures that it is in the same range as the Na. Note that SIMS measures total Na and K concentration, regardless of whether it is mobile or bound. These values are in the same range as those measured by the triangular voltage sweep technique on the same sample (2.1×10^{11} cm^{-2}) and lead us to believe that most of the Na and K is mobile in these oxides.

TABLE 4. SODIUM CONCENTRATION IN HARDENED WET OXIDE 061281 AS MEASURED BY SIMS

Method of measurement	Concentration (atoms cm^{-2}) Under Al dot	Bare oxide
With surface peak included	3.4×10^{11}	4.6×10^{11}
Without surface peak	2.6×10^{11}	1.7×10^{11}

6.2 Measurements of Si/SiO_2 Interface Stoichiometry by Ion-Scattering Spectrometry (ISS)

Many of the electrical phenomena observed in MOS devices originate from charges located at or near the Si/SiO_2 interface. Hole traps and interface states caused by radiation are no exception. Etch-off measurements have shown hole traps to be within 100 Å of the Si interface.[17,18] The stoichiometry of this interface--its nature and its role in the formation of hole traps--has naturally been a subject of some interest. Harrington et al. have shown that it is possible to measure this stoichiometry by the use of ion-scattering spectrometry (ISS).[36,37] We have attempted to do the same for the samples prepared for this study to see if any differences exist between hard and soft oxides.

Low-energy ISS is a useful technique for measuring interface stoichiometry because the low-energy ions that are scattered from the surface in a single atomic collision can be restricted almost entirely to the outermost atomic layer.[36] In Harrington's stoichiometry

[36] W. Harrington, "Low Energy Ion Scattering Spectrometry Studies of Si, SiO_2, and Related Materials," NBS Special Publication 400-23, ARPA/NBS Workshop IV, Washington, DC, Apr. 23-24, 1975.

[37] W. Harrington, R. E. Honig, A. M. Goodman, and R. Williams, Appl. Phys. Lett. 27(12), 644 (1975).

measurements the Si/SiO_2 sample is sputtered with ^4He ions. The energy of the scattered He ion is related to the scattering element in a known relationship.

If the oxygen and silicon ISS signals are plotted as a function of time, the oxygen falls off as the interface is approached while the silicon, of course, increases. Figure 26, in which the signals are plotted as a function of oxide thickness for a hard wet oxide, shows these data. The interfacial region is taken as that point where the oxygen signal falls to 95% of its "bulk" value. The fact that neither signal falls or rises abruptly is not significant. The gradual rise or fall is caused by the rastered beam uncovering several different atomic layers as it sputters a shallow crater into the sample. Even though the signal is mechanically and electronically gated, the crater still has a finite radius of curvature in the region sampled. The important thing to note is that the silicon signal rises before the oxygen falls, an indication of excess silicon. Figure 27 shows the same measurement for a soft wet sample. If the data (solid lines) are interpreted correctly, this soft wet sample has more excess silicon than the hard wet sample, possibly an important difference between the two.

Unfortunately, at present we cannot consider this definitive evidence of more excess silicon in soft oxides. As the figures show, the instrument as it is presently configured produces data with too much scatter (noise) to enable us to arrive at definite conclusions.

6.3 X-Ray Photoelectron Spectroscopy (XPS) Measurements

Radiation-hardened and soft wet- and dry-grown SiO_2 on Si samples was measured by XPS analysis to determine if material stoichiometry near the SiO_2/Si interface could be related to the degree of radiation sensitivity of these oxides. The hole-trap density is typically considerably less than the detectability of our laboratory instrumentation unless trapped charge resides in a very thin sheet near the interface. Even if this were not the case, however, it might be possible to detect interface variations that could be related to hole trapping since, in most oxides, traps are typically filled to only a

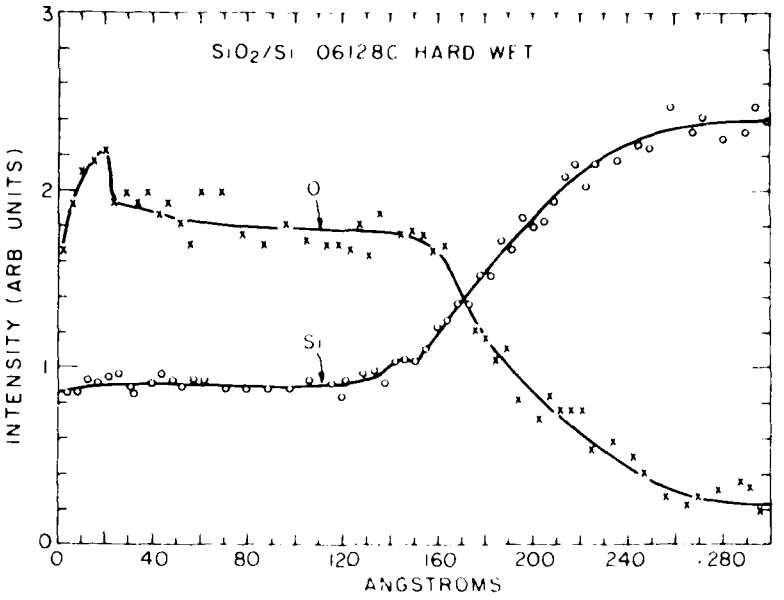

Figure 26. Relative intensity of oxygen and silicon ISS signals as a function of depth in hard wet thin-SiO_2 sample no. 06128C.

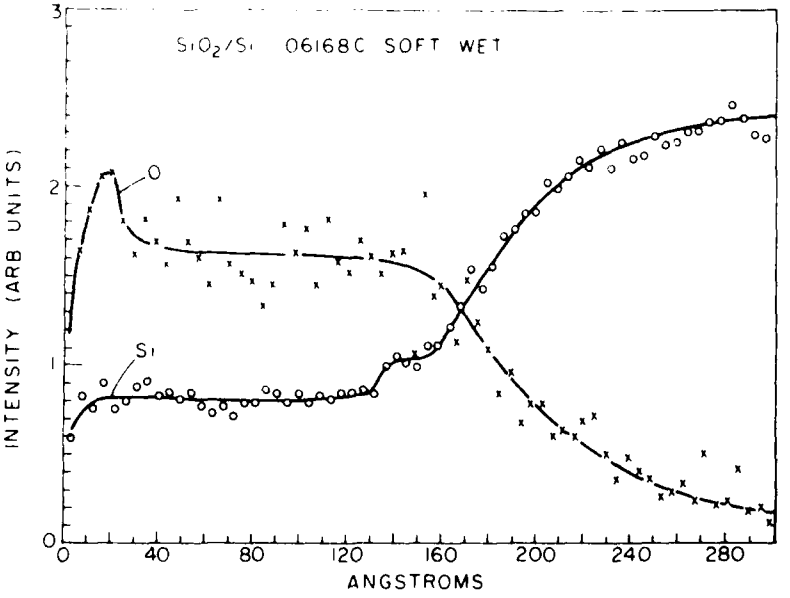

Figure 27. Relative intensity of oxygen and silicon ISS signals as as function of depth in soft wet thin-SiO_2 sample no. 06168C.

small fraction of their actual concentration.[38,39] Therefore, it was decided to study these samples by the use of standard laboratory apparatus.

Two experiments were conducted. In one the stoichiometry of the Si/SiO_2 interface was measured on chemically etched 30-Å SiO_2 films by observation of the chemically shifted Si 2p line. In the other, 100-Å-thick as-grown films were sputter-etched while the shifted Si 2p line structure was profiled as a function of depth.

If the oxide layer on silicon is very thin, photoelectrons emanating from the interfacial region as well as from SiO_2 and the silicon substrate can be detected. For photoelectrons from elemental Si or from Si in SiO_2, Si 2p electrons have been shown to have an escape depth of 23 and 25 Å, respectively.[40] The presence of the chemically shifted Si 2p photoelectron lines other than those representing elemental Si and Si in SiO_2 was used to determine nonstoichiometries near the interface.[40-42] Nonstoichiometry at the interface, detected by surface analysis, has been shown to give rise to electrical properties.[43,44] The following sections summarize experimental results.

[38] J. H. Thomas III, J. Appl. Phys. 45, 835 (1974).
[39] V. J. Kapoor, F. J. Feigl, and S. R. Butler, J. Appl. Phys. 48(2), 739 (1977).
[40] S. I. Raider and R. Flitsch, IBM J. Res. Dev. 22, 294 (1978).
[41] G. Hollinger and Tran Minh Duc, Proc. 7th Int. Conf. Amorphous and Liquid Semiconductors, Edinburgh, Scotland, June 27-July 1, 1977, p. 87.
[42] F. J. Grunthaner and J. Maserjian, in The Physics of SiO_2 and Its Interfaces, ed. by S. T. Pantelides (Pergamon Press, New York, 1978), p. 389.
[43] J. S. Johannessen, W. E. Spicer, and Y. E. Strausser, J. Appl. Phys. 47, 3028 (1976).
[44] The Physics of SiO_2 and Its Interfaces, by S. T. Pantelides (Pergamon Press, New York, 1978), see Chapters VI and VII.

6.3.1 Experimental Techniques

The x-ray photoelectron spectrometer used in this study is based on the double-pass cylindrical mirror analyzer (DPCMA) of Physical Electronic Industries, Inc. The DPCMA is equipped with a coaxially mounted electron gun for electron excitation. Core-level photoionizations were performed with a magnesium K_{α} achromatic x-ray source operated at 400-W input power at an accelerating potential of 10 kV. This source provides a flux of $\sim 10^{13}$ photons cm^{-2} at 1253.6 eV ($K_{\alpha 1,2}$) at the sample surface. Ion cleaning and profiling was accomplished by means of a Physical Electronics Industries ion-gun Model 20-045. This instrument is housed in an ultrahigh-vacuum system equipped with a high-vacuum load-lock sample injection system. Typically, the base pressure in the vacuum system is $5\text{-}8 \times 10^{-10}$ torr. Photoelectrons were detected with a spiraltron electron multiplier and Princeton Applied Research Model 1120/1105 amplifier discriminator and rate meter. Photoelectron statistics were accumulated through the use of an HP Model 5328A counter (Hewlett-Packard) and an Analog Devices digital-to-analog power supply; these devices are software-controlled by an HP 1000 minicomputer and IEEE 488 bus interface.[45] Data are stored on disc during acquisition and are manipulated by data processing and plotting software.

In this study, photoelectron spectra were obtained with the DPCMA operating in a retarding potential mode. Survey spectra were obtained at 200-eV pass energy, and high-resolution spectra at 25-eV pass energy. Statistics for high-resolution spectra were obtained on a 120-point data base for 1.0 s/point and 50 passes (or 50 s/point). High-resolution spectra were deconvolved into Gaussian components after appropriate secondary-electron background removal where required.[46] At 50 s/point, statistics were marginal on the Si 2p photoelectron line. Increasing the number of passes, however, decreases the noise by only the square root of the number of passes.

---

[45] S. H. McFarlane and J. R. Woolston designed this system.
[46] D. A. Shirley, Phys. Rev. B 5(12), 4709 (1972).

Four kinds of samples were measured: hardened and soft wet (pyrogenic steam)-grown and dry-grown oxide films. Growth conditions are described in section 2. These samples were initially grown to 700 Å and some were etched back to 30 Å. The 30-Å-thick samples were prepared to allow the interfacial SiO_2/Si region to be viewed directly by XPS without sputter etching of the material surface. This approach was feasible because of the finite escape depth of the photoionized electrons. Thicker (100 Å) oxides were used for depth-profiling XPS measurements.

6.3.2 Results--30-Å Films

Survey spectra were taken on four chemically thinned samples. A typical spectrum is shown in figure 28. The spectrum shows oxygen, carbon, and silicon. No sodium was detected within experimental limits (~0.1% detectability). The carbon observed on the surface is probably due to physically absorbed CO or CO_2. Because of the film thickness, some of the silicon signal is coming from the substrate. The ratio of Si to O, therefore, is not 1:2, as would be expected in a stoichiometric oxide.[47] Also a trace of nitrogen is observed on each surface. If it is assumed that the CO (or CO_2) is not involved in a chemical bond with the Si and SiO_2 surface, the high-resolution spectra of the Si 2p photoelectron line should give some useful data concerning the interface region.

High-resolution spectra of the silicon 2p and oxygen 1s photoelectron lines were obtained for each sample. Typical silicon 2p and oxygen 1s spectra are shown in figure 29, along with the Gaussian components of the silicon 2p line. The silicon 2p spectrum consists of two major lines, one at 104.35 and the other at 100.0 eV. With this instrument, elemental silicon is observed at a binding energy of 99.4

[47] J. H. Scofield, J. Electron Spectrosc. 8, 129 (1976).

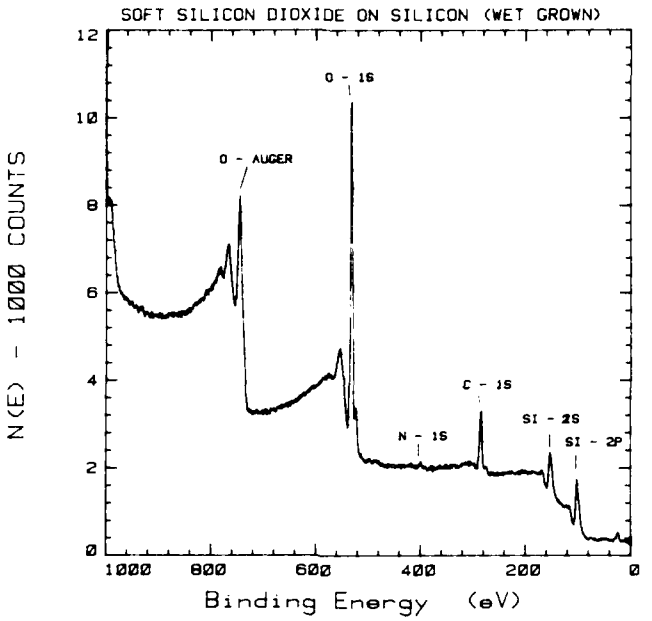

Figure 28. XPS survey spectra of a pyrogenic-steam oxide.

eV.[48] Thus, all the spectral lines are shifted down by 0.6 eV so that the low binding-energy component corresponds to that for elemental silicon. The oxygen 1s line is observed to be a single peak at 533.2 eV (referred to the 99.4-eV Si 2p elemental line) having a full width at half maximum (FWHM) of 1.8 eV. These data were not fitted to a Gaussian curve. The high binding-energy line is due to Si in SiO_2.[40] This is in good agreement with the results of other investigators.[40-42] The FWHM of the Gaussian curves fitted to the main lines (103.8 and 99.4 eV) are 1.8 and 1.35 eV, respectively. The poor fit of the Gaussian to the 99.4 eV is due to the presence of the unresolved spin doublet $2p_{1/2,3/2}$. No attempt was made to deconvolve the doublet since the DPCMA is not capable of providing sufficient resolution. The slight background

[48] J. H. Thomas III and A. M. Goodman, "AES and XPS Studies of Semi-Insulating Polycrystalline Silicon (SIPOS) Layers," J. Electrochem. Soc. 126(10), 1766-70 (1979).

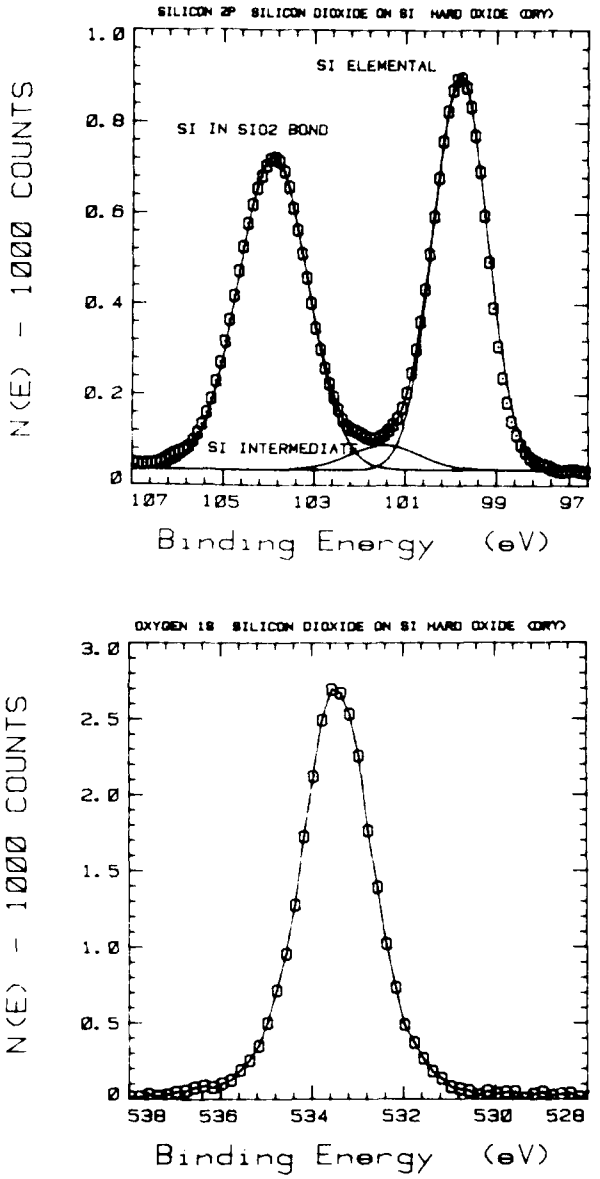

Figure 29. High-resolution spectra of silicon 2p and oxygen 1s lines in hardened dry oxide no. 06128.

slope is an artifact and is due to the presence of a noise fluctuation at the low binding-energy side of the spectrum. The FWHM of the 103.8-eV line (1.8 eV) is in good agreement with the data of other investigators.[40]

A third Gaussian component at 101.1 eV is required to fit the silicon data of figure 29. In other studies, a line due to SiO_x has been observed in the general vicinity of 101 eV (see, for example, Raider and Fletsch[40] and Grunthaner and Maserjian[42]). This component is observed in fitting the data of the four samples with varying amplitudes. These data are summarized in table 5. The amplitudes of the Gaussian components are observed to vary from sample to sample. The major lines at 103.8 and 99.4 eV change amplitude because of a variation in film thickness. In fact, the film thickness can be roughly calculated from the known escape depth for silicon 2p electrons. Using a simple model in which the photoelectron line area is given by[49]

$$dI = N \sigma K F e^{-x/x_o} dx \qquad (13)$$

where I = intensity, N = atom concentration, σ = photoionization cross section, K = spectrometer constant, F = spectrometer transmission, and x_o is the inelastic mean-free-path (IMPF) for photoelectrons, we can calculate the thickness of a film ℓ_f on silicon from the ratio of bound to unbound silicon.[40] The intensity of silicon in SiO_2 is given by

$$I(Si^+) = N(Si^+) \sigma (Si) K F x_o(Si^+) [1 - \exp (-\ell_f/x_o(Si^+)] \qquad (14)$$

and the intensity of silicon from the substrate attenuated by the SiO_2 film of thickness, ℓ, is given by

$$I(Si^o) = N(Si^o) \sigma (Si) K F x_o(Si^o) \exp (-\ell_f/x_o(Si^o) \qquad (15)$$

[49] C. J. Powell, "Recent Pgogress in Quantification of Surface Analysis Techniques" Appl. Surface Sci. 4492 (1980).

TABLE 5. A COMPARISON OF CHEMICALLY THINNED HARDENED AND SOFT SiO_2 ON SILICON GROWN BY WET AND DRY OXIDATION

Sample	$I(Si^+)/I(Si^o)$	ℓ/x_o	Equivalent 101-eV state concentration (at. %)	Carbon concentration (at. %)
Hard-Wet	1.438	1.451	15.2	22.6
Soft-Wet	1.839	1.645	7.8	22.0
Hard-Dry	1.025	1.203	12.9	28.0
Soft-Dry	0.695	0.947	8.8	26.0

If the escape depth (IMPF) of electrons in SiO_2 is assumed to be equal to that of elemental Si, then the ratio $I(Si^+)/I(Si^o)$ can be obtained from equations (14) and (15). Solving this ratio of ℓ, the oxide thickness, yields the following:

$$\frac{\ell}{x_o} = \log e \frac{N(Si^o)}{N(Si^+)} \frac{I(Si^+)}{I(Si^o)} + 1 \qquad (16)$$

where $N(Si^o)/N(Si^+) = 2.273$ and x_o is assumed to be ~ 25 Å.[40] Sample thickness is summarized in table 5.

As noted above, a third Gaussian component required to adequately fit the silicon 2p spectra is observed. The amplitude of this component does not appear to be associated with the observed surface carbon contamination; that is, carbon makes up about 22-29% of the surface concentration from the survey spectra. Therefore, it has been assumed that this peak arises from the immediate interface region. For purposes of analysis it will be assumed that the intermediate state associated with the 101-eV line will be located in the plane of the interface. To compute the "surface concentration" associated with this line, the attenuation due to the oxide thickness must be taken into account. This is simply done by considering escape depth. Rewriting equation (13) in one dimension,

$$dI_o = N_s \delta (x - \ell) \sigma K F e^{-x/x_o} dx \qquad (17)$$

where x_o and σ are values of elemental silicon. Integrating this expression, the intermediate state intensity is given by

$$I_D = N_s \sigma K F x_o e^{-\ell/x_o} \qquad (18)$$

where $I_D(\infty) = N_s K F x_o$ is the intensity of the unattenuated line. By use of the known ℓ/x_o ratio from table 5, the corrected Gaussian component intensity is obtained. These data are summarized in table 5.

6.3.3 Results--100-Å Films

XPS sputter profiling was performed on 100-Å radiation-hardened and soft wet oxides to attempt to study the stoichiometry at the SiO_2-Si interface. Profiling was performed at a rate of 1.84 nm/min by means of 1 keV argon ions (at 5×10^{-5} torr argon pressure). Data were obtained in a step-by-step fashion by sputtering and then evacuating the vacuum system after sputtering. Immediately after sputtering, contaminants in the vacuum system may absorb on the freshly formed silicon surface. This can cause an apparent increase in the density of intermediate states in the Si 2p spectrum.[43,48] By determining the normalized area of the Gaussian components of the silicon 2p line, a depth profile was obtained for bound silicon in SiO_2(Si^+), elemental silicon (Si^o), and intermediate oxides (Si^I). These data are plotted in figure 30 as a function of sputter time in minutes. Equation (16) and the known SiO_2 sputter rate of 1.84 nm/min were used to calculate the thickness of the hardened and soft oxides, 86 and 99 Å, respectively. The 10-90% uncorrected interface width was 78 Å for both samples. This does not include the effect of the difference in the ratio of the sputter rates (1.34) in SiO_2 and Si.[50] This width is larger than the one normally observed at the SiO_2/Si interface by Auger electron spectroscopy, indicating that the sputter spot is not large enough or

[50] J. L. Vossen and E. B. Davidson, J. Electrochem. Soc. 119, 1708 (1972).

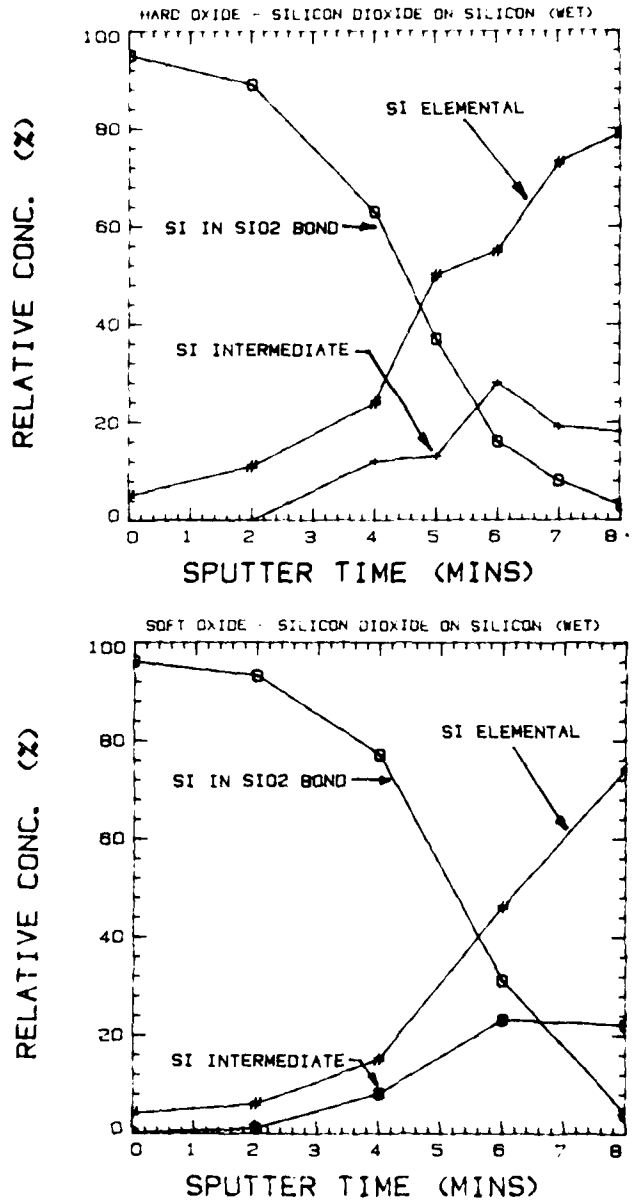

Figure 30. Sputtered depth profiles of elemental silicon, bound silicon, and intermediate-state silicon for hardened wet oxide no. 06128 and soft wet oxide no. 06168.

uniform enough at the DPCMA focus in the XPS mode. The total contribution of the intermediate states is also shown. The Gaussian component is typically at 100.6 and 101.7 eV. Bond concentration seems to peak near the SiO_2/Si interface to about 24% in each sample.

Table 6 summarizes the binding energies of the Gaussian components for each sample for Si^o at 99.4 eV. As reported by Grunthaner and Maserjian,[42] the binding energy of the Si^+ peak shifts toward that of Si^o. The intermediate states (Si^I) occur at (1) $\Delta E_B \tilde{=} 2.4$ eV and (2) $\Delta E_B \tilde{=} 1.2$ eV. It is known that sputtering may introduce states that are not normally observed on unsputtered samples. Therefore, it is believed that part of this bond concentration is caused by sputtering and subsequent additional oxidation due to vacuum exposure during pumpdown from the sputtering pressure. Qualitatively, however, the intermediate-state density appears somewhat larger in the hardened than in the soft oxide (28 and 22 %, respectively; see fig. 30). Further studies are required to clarify the observed difference. One should also include in this analysis the effect of escape depth and damage range at each point in the sputter depth profile.

TABLE 6. BINDING ENERGIES OF THE GAUSSIAN COMPONENTS FITTED TO THE SILICON 2p PHOTOELECTRON LINE AS A FUNCTION OF SPUTTER TIME FOR HARDENED AND SOFT WET OXIDES

	Shift in binding energy* (eV)					
	Soft oxide			Hardened oxide		
Time (min)	Si^+	Si^I (1)	Si^I (2)	Si^+	Si^I (1)	Si^I (2)
0	4.5(1.8)	-	-	4.4(1.7)	-	-
2	4.5(2.1)	2.35(2.0)	-	4.5(2.3)	-	-
4	4.4(2.2)	2.3(2.4?)	1.2(2.4?)	4.05(2.3)	-	1.35(2.4)
6	4.05(2.3)	2.15(2.3)	1.15(2.3)	3.85(2.3)	2.35(2.3)	1.15(2.3)
8	3.83(2.3)	-	1.2(2.3)	-	2.65(2.3)	0.95(2.3)

*FWHM given in parentheses; S^I = intermediate-state silicon.

6.3.4 Conclusions

XPS measurements of chemically thinned oxides and sputter-profiled oxides show measurable differences in the interfacial nonstoichiometric silicon 2p photoionization lines. These intermediate lines are shifted by 2.4 and 1.2 eV from the elemental silicon line at 99.4 eV in the sputter depth-profiled samples. Chemically thinned oxides show an intermediate state shifted by 1.7 eV, that is, midway between the chemical shifts of the sputtered films. On using Raider and Flitsch's expression relating the chemical state of the silicon with the observed chemical shift in the silicon 2p line[40] (that is, in SiO_x), one obtains $\Delta E_B = 2.2x$ where $x = 0.77$ for $\Delta E_B = 1.7$ eV, and $x = 1.1$ and 0.55 for $\Delta E_B = 2.4$ and 1.2 eV, respectively. The actual difference between ΔE_B (chemical etch) and ΔE_B (sputter) is due to ion-damage effects that are presently not well understood.

The concentrations of the intermediate state in both experiments show that the hardened oxide has a state density a few percent larger than that of the soft oxide. Because of the poor experimental control of the samples studied (e.g., air exposure after etching), it is not clear if the difference ($\sim$1%) between the soft oxides is significant. However, it is interesting to note that electrical measurements show the difference between the hole-trap density of the hardened and the soft oxides to be significantly larger in the wet than in the dry oxides. The intermediate-state-density ratio (hard/soft) is larger for the wet than for the dry oxide (1.95 vs 1.46, respectively). These electrically unidentified states may act as compensation for the observed hole traps even though they are observed at (surface) concentrations of $\sim$10%. If these states are dispersed in the interface region, much lower bulk densities can be expected. If the states are electrically active, it is unlikely that more than a few percent of the measured state density will be involved in trapping or compensation.[38,39]

This study has shown that XPS can be used to reveal core correlations between radiation hardness and processing. Further studies, based on more sophisticated experimental procedures should be initiated to clarify and more fully characterize the results of this first study

in which standard XPS facilities were employed. In addition, a detailed study of Auger electron spectroscopy for sputter-depth-profiled hardened and soft oxides may also lead to a greater understanding of the effect of processing on radiation hardness.

7. SUMMARY

Dry- and wet(pyrogenic steam)-grown thermal oxide silicon wafers have been oxidized for several investigations concerning the radiation hardness of thermal SiO_2 MOS devices. These oxides were grown under conditions known to produce state-of-the-art hardened oxides as well as very soft oxides. The purpose of this investigation was to try to characterize the various oxides electrically and chemically to see if a better understanding of the basic mechanisms responsible for hole trapping in SiO_2 could be obtained.

Electrical measurements consisted of high-frequency and quasi-static capacitance voltage (CV), triangular voltage sweep (TVS), and thermally stimulated current (TSC) measurements. Hole traps were filled either by 1-MeV electron irradiation or 10.2-eV vacuum ultraviolet (VUV) irradiation.

Preirradiation TVS measurements at 300°C showed that these oxides contain mobile ions with densities ranging from 3.5×10^{10} cm^{-2} to about 1.5×10^{12} cm^{-2}. Although we have shown what appears to be mobile-ion movement under VUV irradiation, there is no correlation between the radiation hardness of soft and hardened oxides and their measured mobile-ion concentrations. In fact, hardened dry-oxide wafer 06128L had the highest mobile-ion concentration. In addition, in some of the thick-metal capacitors the ions are evidently distributed in a laterally non-uniform manner because the CV curve after stressing has a long shifted "tail" and is hardly shifted at all along the rest of the curve. TVS measurements show peaks that are believed to indicate the presence of Na and K. TSC measurements also show two peaks after an initial positive-bias stress to the capacitor. The location of these peaks at 335 and 535 K corresponds to the location of peaks previously measured in deliberately contaminated samples containing Na and K, respectively.

On some thin-metal wet-oxide capacitors a preirradiation slow-trapping instability was observed. TVS and TSC measurements have led us to conclude that the slow trapping is due to the field emission of electrons from neutral traps, not hole injection. This may be caused by water vapor or organic vapors from the plastic boxes used to store the capacitor wafers.

The thermal-annealing measurements of irradiated MOS capacitors gave varied, but quite interesting, results. Dry-oxide TSC spectra show a gradual increase from 300 to 600 K with no pronounced structure. One exception was a thin-metal capacitor that showed a postirradiation TSC peak at 335 K. Wet oxides exhibit two distinct types of behavior, depending on whether preirradiation thermal behavior is dominated by slow trapping or mobile ions. Those wet-oxide capacitor wafers whose behavior before irradiation is mostly mobile-ion dominated show post-irradiation TSC spectra with distinct peaks at 335 and 585 K, the peaks previously identified as representing Na and K. TVS measurements before and after irradiation show no increase in mobile-ion density. We conclude, therefore, that the irradiation and/or hole flux has moved mobile ions from the Al to the Si interface. Additional TVS measurements also indicate that holes are probably trapped near ions and that detrapping occurs when the ions start to move from one interface to the other. The presence of large densities of ions may distort the local field and could explain the apparent release of holes in a manner resembling that in which mobile ions are released during TSC and TVS measurements.

Those wet-oxide wafers with capacitors having slow-trapping-dominated preirradiation behavior show quite different results. Pre- and postirradiation TSC spectra from identical capacitors from the same wafer show that the holes are trapped very shallow in energy with a probable TSC spectrum for the holes peaked around 410 K. However, if a capacitor has been negatively stressed by TSC before irradiation, the postirradiation thermally stimulated current is very small until near 600 K, and then begins to peak. The incomplete relaxation of the CV shift also indicated that the hole traps are only partially emptied. Although the emptying of the neutral electron traps by negative TSC stressing radically changed the thermal-annealing behavior of trapped

holes, it apparently did not affect the radiation hardness. We believe that hole trapping in these oxides proceeds through an intermediate state (which is not affected by the field emission center) to a final state whose energy depends upon the occupancy of the field emission center.

In attempts to obtain analytical measurements for these oxides we used ion-scattering spectroscopy (ISS), x-ray photoelectron spectroscopy (XPS), and secondary-ion mass spectrometry (SIMS).

Measurements of the interfacial stoichiometry were made with both ISS and XPS. ISS results show a slightly wider "excess silicon" region for the soft wet than for the hardened wet oxide. However, the data contain a large amount of scatter and thus might be interpreted differently than was done in figures 26 and 27. XPS measurements show the presence of interfacial nonstoichiometric silicon in all oxide types. This intermediate-state density is larger in the hardened than in the soft oxides. These states may act as a type of compensation for the disorder that is probably associated with hole traps.

SIMS analysis of the SiO_2 film shows that the technique is capable of measuring both sodium and hydrogen at fairly low levels. The Na measurements confirm TVS electrical measurements with respect to the density of mobile ions measured. Measurements of hydrogen show that a 1100°C steam oxide sample contains a background of hydrogen at a concentration of 8×10^{19} cm^{-3}. This suggests that hydrogen may play a greater role in electrical phenomena in SiO_2 than was thought at one time.

REFERENCES

1. K. Aubuchon, IEEE Trans. Nucl. Sci. NS-18, 117 (1971).
2. G. Derbenwick and B. Gregory, IEEE Trans. Nucl. Sci. NS-22, 2151 (1975).
3. G. W. Hughes and R. J. Powell, "Radiation and Charge Transport in SiO_2," Final Report prepared under Contract N00014-74-C-0185 for Office of Naval Research, May 1976.
4. G. W. Hughes, "Radiation and Charge Transport in SiO_2," Final Report prepared under Contract N000A-74-C-0185 for Office of Naval Research, Feb. 1977.
5. B. E. Deal, J. Electrochem. Soc. 121(6), 198C (1974).
6. B. E. Deal, "Charge Effects and Other Properties of the Si/SiO_2 Interface: The Current Understanding," Proc. Third Int. Symp. Silicon Materials Science and Technol. 1977, p. 276.
7. A. K. Sinha and T. E. Smith, Solid-State Electron. 21(3), 531 (1978).
8. S. R. Hofstein and G. Warfield, Solid-State Electron. 8, 321 (1965).
9. M. Kuhn, Solid-State Electron. 13, 873 (1970).
10. M. Kuhn and D. J. Silversmith, J. Electrochem. Soc. 118(6), 966 (1971).
11. N. J. Chou, J. Electrochem. Soc. 118(4), 601 (1971).
12. G. F. Derbenwick, J. Appl. Phys. 48(3), 1127 (1977).
13. P. Kelley and P. Braunlick, Phys. Rev. B 1, 1587 (1970).
14. J. G. Simmons, G. W. Taylor, and M. C. Tam, Pnys. Rev. B 7(8), 3714 (1973).
15. D. J. DiMaria, in The Physics of SiO_2 and Its Interfaces, ed. by S. T. Pantelides (Pergamon Press, New York, 1978), p. 160.
16. G. W. Hughes, "Radiation Effects on the Electrical Properties of MOS Device Materials," Final Rept. prepared under Contract DAAG39-76-C-0088 for Defense Nuclear Agency, Feb. 1978.
17. R. J. Powell and G. F. Derbenwick, IEEE Trans. Nucl. Sci. NS-18(6), 10 (1971).
18. R. J. Powell and G. W. Hughes, "Radiation and Charge Transport in SiO_2," Final Rept. prepared under Contract N00014-74-C-0185 for Office of Naval Research, 31 Jan. 1975.
19. R. J. Powell and M. Morad, J. Appl. Phys. 49(4), 2499 (1978).

20. E. H. Nicollian, J. Vac. Sci. Technol. 14(5), 1112 (1977).
21. H. Nakayama, Y. Osada, and M. Shindo, J. Electrochem. Soc. 125(8), 1302 (1978).
22. M. Schulz and E. Klausmann, J. Phys. D. (Appl. Phys.) 18, 169 (1979).
23. M. Lenzlinger and E. H. Snow, J. Appl. Phys. 40, 278 (1969).
24. Z. Weinberg, W. Johnson, and M. Lampert, J. Appl. Phys. 47(1), 248 (1976).
25. J. G. Simmons, Phys. Rev. 155, 657 (1967).
26. P. C. Arnett and N. Klein, J. Appl. Phys. 46, 1400 (1975).
27. A. K. Jonscher, Thin Solid Films 1, 213 (1967).
28. M. H. Woods and R. Williams, J. Appl. Phys. 47(3), 1082 (1976).
29. J. Repace, IEEE Trans. Nucl. Sci. NS-24(6), 2088 (1977).
30. J. Repace, IEEE Trans. ED-25(4), 492 (1978).
31. P. Nauta and M. Hillen, J. Appl. Phys. 49(5), 2962 (1978).
32. C. W. Magee, W. L. Harrington, and R. E. Honig, Rev. Sci. Instrum. 49(4), 477 (1978).
33. A. G. Revesz, J. Electrochem. Soc . 126(1), 122 (1979).
34. C. W. Magee and W. L. Harrington, Appl. Phys. Lett. 33(2), 193 (1978).
35. W. Marciniak and H. M. Przewlocki, Phys. Status Solidi A 24, 359 (1974).
36. W. Harrington, "Low Energy Ion Scattering Spectrometry Studies of Si, SiO_2, and Related Materials," NBS Special Publication 440-23, ARPA/NBS Workshop IV, Washington, DC, Apr. 23-24, 1975.
37. W. Harrington, R. E. Honig, A. M. Goodman, and R. Williams, Appl. Phys. Lett. 27(12), 644 (1975).
38. J. H. Thomas III, J. Appl. Phys. 45, 835 (1974).
39. V. J. Kapoor, F. J. Feigl, and S. R. Butler, J. Appl. Phys. 48(2), 739 (1977).
40. S. I. Raider and R. Flitsch, IBM J. Res. Dev. 22, 294 (1978).
41. G. Hollinger and Tran Minh Duc, Proc. 7th Int. Conf. Amorphous and Liquid Semiconductors, Edinburgh, Scotland, June 27-July 1, 1977, p. 87.
42. F. J. Grunthaner and J. Maserjian, in The Physics of SiO_2 and Its Interfaces, ed. by S. T. Pantelides (Pergamon Press, New York, 1978), p. 389.

43. J. S. Johannessen, W. E. Spicer, and Y. E. Strausser, J. Appl. Phys. 47, 3028 (1976).

44. The Physics of SiO_2 and Its Interfaces, ed. by S. T. Pantelides (Pergamon Press, New York, 1978), see Chapters VI and VII.

45. S. H. McFarlane and J. R. Woolston designed this system.

46. D. A. Shirley, Phys. Rev. B 5(12), 4709 (1972).

47. J. H. Scofield, J. Electron Spectrosc. 8, 129 (1976).

48. J. H. Thomas III and A. M. Goodman, "AES and XPS Studies of Semi-Insulating Polycrystalline Silicon (SIPOS) Layers," J. Electrochem. Soc. 126(10), 1766-70 (1979).

49. C. J. Powell, "Recent Progress in Quantification of Surface Analysis Techniques," Appl. Surface Sci. 4, 492 (1980).

50. J. L. Vossen and E. B. Davidson, J. Electrochem. Soc. 119, 1708 (1972).

DISTRIBUTION LIST

051 DATE 25/04/80

DEPARTMENT OF DEFENSE

ASSISTANT TO THE SECRETARY OF DEFENSE
ATOMIC ENERGY
WASHINGTON, DC 20301
ATTN EXECUTIVE ASSISTANT

DIRECTOR
COMMAND & CONTROL TECHNICAL CENTER
DEPARTMENT OF DEFENSE
WASHINGTON, DC 20301
ATTN C-362 C AOKINS

DIRECTOR
DEFENSE ADVANCED RSCH PROJ AGENCY
1400 WILSON BLVD
ARLINGTON, VA 22209
(DESIRES ONLY ONE COPY TO LIBRARY)
ATTN J FRASER

COMMANDER
DEFENSE ELECTRONIC SUPPLY CENTER
1507 WILMINGTON PIKE
DAYTON, OH 45444
ATTN DEC-ESA

DIRECTOR
DEFENSE LOGISTICS AGENCY
CAMERON STATION
ALEXANDRIA, VA 22314
ATTN DLA-QSL J SLATTERY
ATTN DLA-SE

DEFENSE MATERIAL SPECIFICATIONS & STANDARD OFFICE
3320 DUKE STREET
ALEXANDRIA, VA 22314
ATTN L COX

DIRECTOR
DEFENSE NUCLEAR AGENCY
WASHINGTON, DC 20305
01CY ATTN RAEV M KEMP
01CY ATTN RAEV A KUBO
01CY ATTN RAEV/W MOHR
01CY ATTN DDST
04CY ATTN TITL

DEFENSE TECHNICAL INFORMATION CENTER
CAMERON STATION
ALEXANDRIA, VA 22314
(12 IF OPEN PUB, OTHERWISE 2 - NO WNINTEL)
12CY ATTN DD
ATTN DTIC-DDA (2)

COMMANDER
FIELD COMMAND
DEFENSE NUCLEAR AGENCY
KIRTLAND AFB, NM 87115
01CY ATTN FCPR

CHIEF
FIELD COMMAND
DEFENSE NUCLEAR AGENCY
LIVERMORE DIVISION
P O BOX 808 L-317
LIVERMORE, CA 94550
01CY ATTN FCPRL

DIRECTOR
NATIONAL SECURITY AGENCY
FORT GEORGE G MEADE, MD 20755
01CY ATTN P DEROY
01CY ATTN G DAILY
01CY ATTN T BROWN

COMMANDANT
NATO SCHOOL (SHAPE)
APO NEW YORK, NY 09172
01CY ATTN U S DOCUMENTS OFFICER

UNDER SECY OF DEF FOR RSCH & ENGRG
DEPARTMENT OF DEFENSE
WASHINGTON, DC 20301
01CY ATTN STRATEGIC & SPACE SYSTEMS (OS)

051

DEPARTMENT OF ARMY DATE 25/04/80

COMMANDER
ABERDEEN PROVING GROUND
DEPARTMENT OF THE ARMY
ABERDEEN PROVING GROUND, MD 21005
01CY ATTN S HARRISON

DIRECTOR
BMD ADVANCED TECHNOLOGY CENTER
DEPARTMENT OF THE ARMY
P O BOX 1500
HUNTSVILLE, AL 35807
01CY ATTN ATC-O F HOKE
01CY ATTN ATC-T

COMMANDER
BMD SYSTEMS COMMAND
DEPARTMENT OF THE ARMY
P O BOX 1500
HUNTSVILLE, AL 35807
01CY ATTN BMDSC-HW P DE KALB

DEPARTMENT OF ARMY

DEPUTY CHIEF OF STAFF FOR RSCH DEV & ACQ
DEPARTMENT OF THE ARMY
WASHINGTON, DC 20310
01CY ATTN ADVISOR FOR SDA ANALYSIS (M GALE)

COMMANDER (3)
HARRY DIAMOND LABORATORIES
DEPARTMENT OF THE ARMY
2800 POWDER MILL ROAD
ADELPHI, MD 20783
(CNWDI-INNER ENVELOPE: ATTN: DELHD-RBH)
01CY ATTN DELHD-N-RBH J HALPIN
01CY ATTN DELHD-N-RBH H EISEN
01CY ATTN DELHD-N-RBH
01CY ATTN DELHD-N-P
01CY ATTN DELHD-N-RBC J MCGARRITY
01CY ATTN DELHD-N-P F BALICKI
ATTN LIBRARY (3)
ATTN EDITORIAL COMMITTEE (CHAIRMAN)
ATTN BRANCH 013
ATTN PUBLIC AFFAIRS OFFICER (HDL)
ATTN BRANCH 04100 (RECORD COPY)

COMMANDER
U S ARMY ARMAMENT RESEARCH & DEVELOPMENT COMMAND
DOVER, NJ 07801
01CY ATTN DRDAR-LCA-PD

U S ARMY COMMUNICATIONS R&D COMMAND
FORT MONMOUTH, NJ 07703
01CY ATTN D HUEWE

COMMANDER
U S ARMY MATERIEL & MECHANICS RSCH CTR
WATERTOWN, MA 02172
(ADDRESS CNWDI: ATTN: DOCUMENT CONTROL FOR:)
01CY ATTN DRXMR-HP J HOFMANN

COMMANDER
U S ARMY MISSILE COMMAND
REDSTONE ARSENAL, AL 35809
03CY ATTN RSIC

COMMANDER
U S ARMY NUCLEAR & CHEMICAL AGENCY
7500 BACKLICK ROAD
BUILDING 2073
SPRINGFIELD, VA 22150
(DESIRES ONLY 1 CY TO LIBRARY)
01CY ATTN LIBRARY

COMMANDER
WHITE SANDS MISSILE RANGE
DEPARTMENT OF THE ARMY
WHITE SANDS MISSILE RANGE, NM 88002
01CY ATTN STEWS-TE-AN T LEURA
01CY ATTN STEWS-TE-AN M SQUIRES

DEPARTMENT OF NAVY

COMMANDER
NAVAL AIR SYSTEMS COMMAND
WASHINGTON, DC 21360
01CY ATTN AIR 350F

COMMANDER
NAVAL ELECTRONIC SYSTEMS COMMAND
WASHINGTON, DC 20360
01CY ATTN CODE 5045.11 C SUMAN

COMMANDER
NAVAL OCEAN SYSTEMS CENTER
SAN DIEGO, CA 92152
01CY ATTN CODE 4471 (TECH LIB)

SUPERINTENDENT
NAVAL POSTGRADUATE SCHOOL
MONTEREY, CA 93940
(DESIRES NO CNWDI DOCUMENTS)
01CY ATTN CODE 0142 LIBRARY
01CY ATTN CODE 1424 LIBRARY

COMMANDING OFFICER
NAVAL RESEARCH LABORATORY
WASHINGTON, DC 20375
(RD & RP/N ATTN CODE 1221 FOR E
SRD ATTN CODE 2628
01CY ATTN CODE 5213 J KILLIANY
01CY ATTN CODE 4701 J BROWN
01CY ATTN CODE 5210 J DAVEY
01CY ATTN CODE 6601 F WOLICKI
01CY ATTN CODE 6650 A ASMENSON
01CY ATTN CODE 6600 J MCELLINNEY
01CY ATTN CODE 6627 C GUENZER
01CY ATTN CODE 5216 H HUGHES

DEPARTMENT OF NAVY

COMMANDER
NAVAL SEA SYSTEMS COMMAND
WASHINGTON, DC 20362
01CY ATTN SEA-06J P LANE

OFFICER IN CHARGE
NAVAL SURFACE WEAPONS CENTER
WHITE OAK LABORATORY
SILVER SPRING, MD 20910
01CY ATTN CODE F30
01CY ATTN CODE F31

COMMANDER
NAVAL WEAPONS CENTER
CHINA LAKE, CA 93555
01CY ATTN CODE 233 (TECH LIB)

COMMANDING OFFICER
NAVAL WEAPONS EVALUATION FACILITY
KIRTLAND AIR FORCE BASE
ALBUQUERQUE, NM 87117
01CY ATTN CODE AT-6

COMMANDING OFFICER
NAVAL WEAPONS SUPPORT CENTER
CRANE, IN 47522
01CY ATTN CODE 7024 T ELLIS
01CY ATTN CODE 70242 J MUNARIN
01CY ATTN CODE 7024 J RAMSEY

OFFICE OF NAVAL RESEARCH
ARLINGTON, VA 22217
01CY ATTN CODE 427 L COOPER
01CY ATTN CODE 220 D LEWIS

OFFICE OF THE CHIEF OF NAVAL OPERATIONS
WASHINGTON, DC 20350
01CY ATTN OP 985E

DIRECTOR
STRATEGIC SYSTEMS PROJECT OFFICE
DEPARTMENT OF THE NAVY
WASHINGTON, DC 20376
01CY ATTN NSP-230 D GOLD
01CY ATTN NSP-2701 J PITSENBERGER
01CY ATTN NSP-27331 P SPECTOR
01CY ATTN NSP-2015

DEPARTMENT OF THE AIR FORCE

AIR FORCE AERO-PROPULSION LABORATORY
WRIGHT-PATTERSON AFB, OH 45433
01CY ATTN POD P STOVER

AIR FORCE GEOPHYSICS LABORATORY
HANSCOM AFB, MA 01731
01CY ATTN SULL S-29
01CY ATTN SULL

AIR FORCE INSTITUTE OF TECHNOLOGY
AIR UNIVERSITY
WRIGHT-PATTERSON AFB, OH 45433
(DOES NOT DESIRE CLASSIFIED DOCUMENTS)
01CY ATTN END J BRIDGEMAN

AIR FORCE MATERIALS LABORATORY
WRIGHT-PATTERSON AFB, OH 45433
01CY ATTN LTE
01CY ATTN LPO R HICKMOTT

HEADQUARTERS
AIR FORCE SYSTEMS COMMAND
ANDREWS AFB
WASHINGTON, DC 20334
01CY ATTN DLCA
01CY ATTN DLW
01CY ATTN DLCAM T SEALE
01CY ATTN XRLA P STEAD
01CY ATTN MNNG
01CY ATTN MNNF J TUCKER

COMMANDER
FOREIGN TECHNOLOGY DIVISION, AFSC
WRIGHT-PATTERSON AFB, OH 45433
01CY ATTN TQTD B BALLARD
01CY ATTN PDJV

HEADQUARTERS SPACE DIVISION
AIR FORCE SYSTEMS COMMAND
POST OFFICE BOX 92960
WORLDWAY POSTAL CENTER
LOS ANGELES, CA 90009
01CY ATTN C KELLY

HEADQUARTERS SPACE DIVISION/AQ
AIR FORCE SYSTEMS COMMAND
POST OFFICE BOX 92960
WORLDWAY POSTAL CENTER
LOS ANGELES, CA 90009
01CY ATTN AQM
01CY ATTN AQT W PLASKEY

DSI DATE 25/04/80

DEPARTMENT OF THE AIR FORCE

HEADQUARTERS SPACE DIVISION/DY
AIR FORCE SYSTEMS COMMAND
POST OFFICE BOX 92960
WORLDWAY POSTAL CENTER
LOS ANGELES, CA 90009
(TECHNOLOGY)
01CY ATTN DYS

HEADQUARTERS SPACE DIVISION/SZ
AIR FORCE SYSTEMS COMMAND
POST OFFICE BOX 92960
WORLDWAY POSTAL CENTER
LOS ANGELES, CA 90009
(SPACE DEFENSE SYSTEMS)
01CY ATTN SZJ R DAVIS

COMMANDER
ROME AIR DEVELOPMENT CENTER, AFSC
GRIFFISS AFB, NY 13441
(DESIGNATED [illegible])
01CY ATTN [illegible]
01CY ATTN [illegible]

COMMANDER
ROME AIR DEVELOPMENT CENTER, AFSC
HANSCOM AFB, MA 01731
01CY ATTN ESR P VAIL
01CY ATTN ETS R DOLAN
01CY ATTN ESR W SHEDD
01CY ATTN ESE A KAHAN
01CY ATTN ESER R BUCHANAN

STRATEGIC AIR COMMAND/XPFS
DEPARTMENT OF THE AIR FORCE
OFFUTT AFB, NB 69113
01CY ATTN XPFS M CARRA

AIR FORCE TECHNICAL APPLICATIONS CENTER
PATRICK AFB, FL 32925
01CY ATTN TAF

AIR FORCE WEAPONS LABORATORY, AFSC
KIRTLAND AFB, NM 87117
01CY ATTN [illegible]
01CY ATTN [illegible]
[illegible]

DSI DATE 25/04/80

DEPARTMENT OF THE AIR FORCE

AIR FORCE WRIGHT AERONAUTICAL LABORATORIES
WRIGHT-PATTERSON AFB, OH 45433
01CY ATTN TEA R CONKLIN
01CY ATTN DH

COMMANDER
AIR LOGISTICS COMMAND
DEPARTMENT OF THE AIR FORCE
HILL AFB, UT 84406
01CY ATTN MMEDO
01CY ATTN DD-ALC/MM R BLACKBURN
01CY ATTN MMETH

BALLISTIC MISSILE OFFICE/MN
AIR FORCE SYSTEMS COMMAND
NORTON AFB, CA 92409
(MINUTEMAN)
01CY ATTN MNNL

DSI DATE 25/04/80

DEPARTMENT OF ENERGY

DEPARTMENT OF ENERGY
ALBUQUERQUE OPERATIONS OFFICE
P O BOX 5400
ALBUQUERQUE, NM 87115
01CY ATTN WSSB

DSI DATE 25/04/80

OTHER GOVERNMENT

CENTRAL INTELLIGENCE AGENCY
WASHINGTON, DC 20505
01CY ATTN OSI/RD
01CY ATTN OSI/MTD A PADGETT

DEPARTMENT OF COMMERCE
NATIONAL BUREAU OF STANDARDS
WASHINGTON, DC 20234
(ALL CORRES: ATTN SEC OFFICER FOR)
01CY ATTN W BULLIS
01CY ATTN K GALLOWAY
01CY ATTN S CHAPPELL
01CY ATTN R SCACE
01CY ATTN J MAYO-WELLS
01CY ATTN J FRENCH
01CY ATTN J HUMPHREYS

USL DATE 25/04/80

OTHER GOVERNMENT

NASA
GODDARD SPACE FLIGHT CENTER
GREENBELT, MD 20771
  01CY ATTN J ADOLPHSEN
  01CY ATTN V DANCHENKO

NASA
GEORGE C MARSHALL SPACE FLIGHT CENTER
HUNTSVILLE, AL 35812
  01CY ATTN M NOWAKOWSKI
  01CY ATTN L HANEFER
  01CY ATTN EB32

NASA
600 INDEPENDENCE AVENUE, SW
WASHINGTON, DC 20546
  01CY ATTN J MURPHY

NASA
LEWIS RESEARCH CENTER
21000 BROOKPARK ROAD
CLEVELAND, OH 44135
  01CY ATTN M RAUDORF

NASA
AMES RESEARCH CENTER
MOFFETT FIELD, CA 94035
  01CY ATTN C DEVOLAD

USL DATE 25/04/80

DEPARTMENT OF DEFENSE CONTRACTORS

ADVANCED MICRODEVICES, INC.
901 THOMPSON PLACE
SUNNYVALE, CA 94086
  01CY ATTN J SCHLAGETER

ADVANCED RESEARCH & APPLICATIONS CORP.
1223 E ARQUES AVENUE
SUNNYVALE, CA 94086
  01CY ATTN R ARMISTEAD
  01CY ATTN I PALOLTI

AEROJET ELECTRO-SYSTEMS CO.
P O BOX 296, 1100 W HOLLYVALE DRIVE
AZUSA, CA 91702
  01CY ATTN T HANCOME

AEROSPACE CORP.
P O BOX 92957
LOS ANGELES, CA 90009
  01CY ATTN R CROLIUS
  01CY ATTN S BOWER
  01CY ATTN D FRASER

AEROSPACE INDUSTRIES ASSOC. OF AMERICA, INC.
1725 E SALES STREET, NW
WASHINGTON, DC 20036
  01CY ATTN S SIEGEL

BATTELLE MEMORIAL INSTITUTE
505 KING AVENUE
COLUMBUS, OH 43201
  01CY ATTN W THATCHER

BDM CORP.
P O BOX 9274
ALBUQUERQUE, NM 87119
  01CY ATTN R PEACE
  01CY ATTN D ALEXANDER
  01CY ATTN D WUNCH

BENDIX CORP.
NAVIGATION AND CONTROL GROUP
TETERBORO, NJ 07608
  01CY ATTN F MEEDER

BOEING CO.
P O BOX 3707
SEATTLE, WA 98124
  01CY ATTN D EGELKROUT

BOEING CO.
P O BOX 3999
SEATTLE, WA 98124
  01CY ATTN C ROSENBERG
  01CY ATTN I SHIMURA
  01CY ATTN A JOHNSTON
  01CY ATTN W RUMPZA

BURR-BROWN RESEARCH CORP.
P O BOX 11400
TUCSON, AZ 85734
  01CY ATTN H SMITH (UNCLASSIFIED ONLY)

DEPARTMENT OF DEFENSE CONTRACTORS

CALIFORNIA INSTITUTE OF TECHNOLOGY
JET PROPULSION LAB
4800 OAK GROVE DRIVE
PASADENA, CA 91103
01CY ATTN A SHUMKA
01CY ATTN A STANLEY
01CY ATTN W PRICE

CHARLES STARK DRAPER LAB, INC.
555 TECHNOLOGY SQUARE
CAMBRIDGE, MA 02139
01CY ATTN P KELLY
01CY ATTN R SLEETER
01CY ATTN C LAI
01CY ATTN A SCHULTZ
01CY ATTN R REDINGER (LIB)
01CY ATTN R LEDGER
01CY ATTN A FREEMAN

CINCINNATI ELECTRONICS CORP.
2630 GLENDALE-MILFORD RD
CINCINNATI, OH 45241
01CY ATTN C STUMP
01CY ATTN L HAMMOND

CONTROL DATA CORP.
P O BOX 0
MINNEAPOLIS, MN 55440
01CY ATTN J MECHAN
01CY ATTN T FRYE

DENVER, UNIVERSITY OF
COLORADO SEMINARY
DENVER RESEARCH INSTITUTE
P O BOX 10127
DENVER, CO 80210
(ONLY 1 COPY OF CLASS RPTS)
01CY ATTN SEC OFFICER FOR E VENDITTI

E-SYSTEMS, INC.
GARLAND DIVISION
P O BOX 226118
DALLAS, TX 75266
01CY ATTN K REIS

ELECTRONIC INDUSTRIES ASSOCIATION
2001 EYE STREET, NW
WASHINGTON,, DC 20006
01CY ATTN J HESSMAN

EMM CORP.
3883 N 28TH AVENUE
PHOENIX, AZ 85017
01CY ATTN E KOCH

EXP & MATH PHYSICS CONSULT NTL
P O BOX 66331
LOS ANGELES, CA 90066
01CY ATTN T JORDAN

FORD AEROSPACE & COMMUNICATIONS CORP.
FORD & JAMBOREE ROADS
NEWPORT BEACH, CA 92663
01CY ATTN TECHNICAL INFORMATION SERVICES
01CY ATTN J DAVISON

FRANKLIN INSTITUTE
20TH STREET AND PARKWAY
PHILADELPHIA, PA 19103
01CY ATTN R THOMPSON

GARRETT CORP.
2525 W 190TH STREET
TORRANCE, CA 90509
01CY ATTN P WEIR

GENERAL DYNAMICS CORP.
CONVAIR DIVISION
P O BOX 80847
SAN DIEGO, CA 92138
(CLASSIFIED TO CONVAIR TECHNICAL LIBRARY)
01CY ATTN W HANNEN

GENERAL ELECTRIC CO.
AIRCRAFT ENGINE BUSINESS GROUP
EVENDALE PLANT, INT HWY 75 S
CINCINNATI, OH 45215
01CY ATTN R HELLER

GENERAL ELECTRIC CO.
AEROSPACE ELECTRONICS SYSTEMS
FRENCH ROAD
UTICA, NY 13503
01CY ATTN D COLE
01CY ATTN J GIPSON

GENERAL ELECTRIC CO.
P O BOX 5000
BINGHAMTON, NY 13902
01CY ATTN D REDIN

GENERAL ELECTRIC CO.-TEMPO
816 STATE STREET (P O DRAWER QQ)
SANTA BARBARA, CA 93102
01CY ATTN M ESPIG
01CY ATTN DASIAC

DEPARTMENT OF DEFENSE CONTRACTORS

GENERAL ELECTRIC CO.-TEMPO
HUNTINGTON BUILDING, SUITE 300
2560 HUNTINGTON AVENUE
ALEXANDRIA, VA 22303
01CY ATTN DASIAC

GENERAL RESEARCH CORP.
SANTA BARBARA DIVISION
P O BOX 6770
SANTA BARBARA, CA 93111
01CY ATTN TECHNICAL INFORMATION OFFICE
01CY ATTN K HILL

GEORGE C. MESSENGER
CONSULTING ENGINEER
3111 BEL AIR DRIVE, 7-F
LAS VEGAS, NV 89109
01CY ATTN G MESSENGER

GEORGIA INSTITUTE OF TECHNOLOGY
GEORGIA TECH RESEARCH INSTITUTE
ATLANTA, GA 30332
01CY ATTN R CURRY (UNCL ONLY)

GEORGIA INSTITUTE OF TECHNOLOGY
OFFICE OF CONTRACT ADMINISTRATION
ATTN: PSCH SECURITY COORDINATOR
ATLANTA, GA 30332
01CY ATTN RES & SEC COORD FOR H DENNY
(UNCLASS ONLY)

GOODYEAR AEROSPACE CORP.
ARIZONA DIVISION
LITCHFIELD PARK, AZ 85340
01CY ATTN SECURITY CONTROL STATION

GENERAL DYNAMICS CORP.
FORT WORTH DIVISION
P O BOX 748, GRANTS LANE
FORT WORTH, TX 76101
01CY ATTN R FIELDS
01CY ATTN J WOOD

GENERAL ELECTRIC CO.
SPACE DIVISION
VALLEY FORGE SPACE CENTER
P O BOX 8555
PHILADELPHIA, PA 19101
01CY ATTN J ANDREWS
01CY ATTN R CASEY
01CY ATTN J PEDEN

GENERAL ELECTRIC CO.
RE-ENTRY & ENVIRONMENTAL SYSTEMS DIV
P O BOX 7722
3198 CHESTNUT STREET
PHILADELPHIA, PA 19101
01CY ATTN W PATTERSON
01CY ATTN TECHNICAL LIBRARY
01CY ATTN P BENEDICT
01CY ATTN J PALCHEFSKY JR
01CY ATTN R CASEY

GENERAL ELECTRIC CO.
ORDNANCE SYSTEMS
100 PLASTICS AVENUE
PITTSFIELD, MA 01201
01CY ATTN J REIDL

GRUMMAN AEROSPACE CORP.
S OYSTER BAY ROAD
BETHPAGE, NY 11714
01CY ATTN J ROGERS

GTE SYLVANIA, INC.
ELECTRONICS SYSTEMS GRP-EASTERN DIV
77 A STREET
NEEDHAM, MA 02194
01CY ATTN L BLAISDELL
01CY ATTN C THORNHILL
01CY ATTN L PAUPLES

GTE SYLVANIA, INC.
189 B STREET
NEEDHAM HEIGHTS, MA 02194
01CY ATTN H ULLMAN
01CY ATTN J WALDRON
01CY ATTN P FREDRICKSON
01CY ATTN H & V GROUP

HARRIS CORP.
HARRIS SEMICONDUCTOR DIVISION
P O BOX 883
MELBOURNE, FL 32901
01CY ATTN C ANDERSON
01CY ATTN J CORNELL
01CY ATTN T SANDERS

HONEYWELL, INC.
AVIONICS DIVISION
2600 RIDGEWAY PARKWAY
MINNEAPOLIS, MN 55413
01CY ATTN R GUMM

HONEYWELL, INC.
AVIONICS DIVISION
P O BOX 11563
ST PETERSBURG, FL 33733
01CY ATTN C CERULLI

DEPARTMENT OF DEFENSE CONTRACTORS

HONEYWELL, INC.
RADIATION CENTER
2 FORBES ROAD
LEXINGTON, MA 02173
01CY ATTN TECHNICAL LIBRARY

HUGHES AIRCRAFT CO.
CENTINELA AND TEALE
CULVER CITY, CA 90230
01CY ATTN R MCGOWAN
01CY ATTN J SINGLETARY

HUGHES AIRCRAFT CO.
EL SEGUNDO SITE
P O BOX 92919
LOS ANGELES, CA 90009
01CY ATTN E SMITH
01CY ATTN D SHUMAKE
01CY ATTN W SCOTT

IBM CORP.
ROUTE 17C
OWEGO, NY 13827
01CY ATTN T MARTIN
01CY ATTN F TIETSE
01CY ATTN H MATHERS

IIT RESEARCH INSTITUTE
10 W 35TH STREET
CHICAGO, IL 60616
01CY ATTN I MINDEL

INSTITUTE FOR DEFENSE ANALYSES
400 ARMY-NAVY DRIVE
ARLINGTON, VA 22202
01CY ATTN TECH INFO SERVICES

INTEL CORP.
3065 BOWERS AVENUE
MAIL STOP 1-156
SANTA CLARA, CA 95051
01CY ATTN M JORDAN

INTERNATIONAL BUSINESS MACHINE CORP.
THOMAS WATSON RESEARCH CENTER
BOX 218
YORKTOWN HEIGHTS, NY 10598
01CY ATTN J ZIEGLER

INTERNATIONAL TEL & TELEGRAPH CORP.
500 WASHINGTON AVENUE
NUTLEY, NJ 07110
01CY ATTN DEPT 60R
01CY ATTN A RICHARDSON

INTERSIL INC.
3250 SCOTT BOULEVARD
SANTA CLARA, CA 95051
01CY ATTN D MACDONALD

IRT CORP.
P O BOX 81087
SAN DIEGO, CA 92138
01CY ATTN J HARRITY

JAYCOR
1401 CAMINO DEL MAR
DEL MAR, CA 92014
(DESIRES ONLY ONE COPY)
01CY ATTN L SCOTT
01CY ATTN R STAHL
01CY ATTN T FLANAGAN

JOHNS HOPKINS UNIVERSITY
APPLIED PHYSICS LAB
JOHNS HOPKINS ROAD
LAUREL, MD 20810
01CY ATTN P PARTRIDGE

KAMAN SCIENCES CORP.
P O BOX 7463
COLORADO SPRINGS, CO 80933
01CY ATTN M BELL
01CY ATTN J LUBELL

LAWRENCE LIVERMORE LABORATORY
P O BOX 808
LIVERMORE, CA 94550
01CY ATTN DOC CON FOR TECHNICAL
INFORMATION DEPT.

LITTON SYSTEMS, INC.
GUIDANCE & CONTROL SYSTEMS DIVISION
5500 CANOGA AVENUE
WOODLAND HILLS, CA 91364
01CY ATTN G MADDOX
01CY ATTN J RETZLER

LOCKHEED MISSILES & SPACE CO., INC.
3251 HANOVER STREET
PALO ALTO, CA 94304
01CY ATTN J CROWLEY
01CY ATTN J SMITH

DNA 25/04/80

DEPARTMENT OF DEFENSE CONTRACTORS

LOCKHEED MISSILES & SPACE CO., INC.
P O BOX 504
SUNNYVALE, CA 94086
  01CY ATTN F MESSEE
  01CY ATTN C THOMPSON
  01CY ATTN P BENE
  01CY ATTN M SMITH
  01CY ATTN E SMITH
  01CY ATTN D PHILLIPS/DEPT 62-46 BLDG 151

LOS ALAMOS SCIENTIFIC LABORATORY
MAIL STATION 5000
P O BOX 1663
LOS ALAMOS, NM 87545
  01CY ATTN DOC CON FOR J FREED

M.I.T. LINCOLN LAB
P O BOX 73
LEXINGTON, MA 02173
  01CY ATTN P MCKENZIE

MAGNAVOX GOVT & INDLS ELECTRONICS CO.
1313 PRODUCTION ROAD
FORT WAYNE, IN 46808
  01CY ATTN W RICHESON

MARTIN MARIETTA CORP.
P O BOX 5837
ORLANDO, FL 32855
  01CY ATTN W JANOCKO
  01CY ATTN W BROCKETT
  01CY ATTN R SAYNOR
  01CY ATTN H GATES

MARTIN MARIETTA CORP.
P O BOX 179
DENVER, CO 80201
  01CY ATTN E CARTER

MCDONNELL DOUGLAS CORP.
P O BOX 516
ST LOUIS, MO 63166
  01CY ATTN LIBRARY
  01CY ATTN M STITCH
  01CY ATTN J OHM

MCDONNELL DOUGLAS CORP.
5301 BOLSA AVENUE
HUNTINGTON BEACH, CA 92647
  01CY ATTN J HOLMGREN
  01CY ATTN O FITZGERALD

MCDONNELL DOUGLAS CORP.
3855 LAKEWOOD BOULEVARD
LONG BEACH, CA 90846
  01CY ATTN TECHNICAL LIBRARY

MISSION RESEARCH CORP.
P O DRAWER 719
SANTA BARBARA, CA 93102
  (ALL CLASS: ATTN: SEC OFC FOR)
  01CY ATTN C LONGMIRE

MISSION RESEARCH CORP.
EM SYSTEM APPLICATIONS DIVISION
1400 SAN MATEO BLVD, SE, SUITE A
ALBUQUERQUE, NM 87108
  01CY ATTN R PEASE

MISSION RESEARCH CORP.-SAN DIEGO
P O BOX 1209
LA JOLLA, CA 92038
  (VICTOR A J VAN LINT)
  01CY ATTN V VAN LINT
  01CY ATTN J RAYMOND

MITRE CORP.
P O BOX 208
BEDFORD, MA 01730
  01CY ATTN M FITZGERALD

MOTOROLA, INC.
GOVERNMENT ELECTRONICS DIVISION
P O BOX 1417
SCOTTSDALE, AZ 85252
  01CY ATTN A CHRISTENSEN

MOTOROLA, INC.
SEMICONDUCTOR GROUP
P O BOX 2953
PHOENIX, AZ 85062
  01CY ATTN L CLARK
  01CY ATTN R GARDNER

NATIONAL ACADEMY OF SCIENCES
NATIONAL MATERIALS ADVISORY BOARD
2101 CONSTITUTION AVENUE, NW
WASHINGTON, DC 20418
  01CY ATTN R SHANE

NATIONAL SEMICONDUCTOR CORP.
2900 SEMICONDUCTOR DRIVE
SANTA CLARA, CA 95051
  01CY ATTN A LONDON
  01CY ATTN R WANG

DEPARTMENT OF DEFENSE CONTRACTORS

NEW MEXICO, UNIVERSITY OF
ELECTRICAL ENGINEERING & COMPUTER SCIENCE DEPT
ALBUQUERQUE, NM 87131
01CY ATTN H SOUTHWARD

NORTHROP CORP.
NORTHROP RESEARCH & TECHNOLOGY CTR
1 RESEARCH PARK
PALOS VERDES PENINSULA, CA 90274
01CY ATTN J SKOUP
01CY ATTN P EISENBERG
01CY ATTN T JACKSON

NORTHROP CORP.
ELECTRONIC DIVISION
2301 W 120TH STREET
HAWTHORNE, CA 90250
01CY ATTN L ARDOSA

PHYSICS INTERNATIONAL CO.
2700 MERCED STREET
SAN LEANDRO, CA 94577
01CY ATTN DIVISION 6000
01CY ATTN J HUNTINGTON
01CY ATTN J SHEA

R & D ASSOCIATES
P O BOX 9695
MARINA DEL REY, CA 90291
01CY ATTN R POLL
01CY ATTN C MACDONALD
01CY ATTN S ROGERS

RAND CORP.
1700 MAIN STREET
SANTA MONICA, CA 90406
01CY ATTN C CRAIN

RAYTHEON CO.
HARTWELL ROAD
BEDFORD, MA 01730
01CY ATTN J CICCIO

RAYTHEON CO.
528 BOSTON POST ROAD
SUDBURY, MA 01776
01CY ATTN A VAN DOREN
01CY ATTN H FLESCHER

RCA CORP.
GOVERNMENT SYSTEMS DIVISION
ASTRO ELECTRONICS
P O BOX 800, LOCUST CORNER
EAST WINDSOR TOWNSHIP
PRINCETON, NJ 08540
01CY ATTN G BRUCKER (UNCL ONLY)
01CY ATTN V MANCINO

RCA CORP.
GOVERNMENT SYSTEMS DIVISION
MISSILE & SURFACE RADAR
MARNE HIGHWAY & BORTON LANDING RD
MOORESTOWN, NJ 08057
01CY ATTN R KILLION

RCA CORP.
CAMDEN COMPLEX
FRONT & COOPER STREETS
CAMDEN, NJ 08012
01CY ATTN E VAN KEUREN
01CY ATTN J SAULTZ

RCA CORP.
SOMERVILLE PLANT, SOLID STATE DIV
P O BOX 591
SOMERVILLE, NJ 08876
01CY ATTN W ALLEN

RENSSELAER POLYTECHNIC INSTITUTE
P O BOX 965
TROY, NY 12181
01CY ATTN R GUTMANN (UNCLAS ONLY)

RESEARCH TRIANGLE INSTITUTE
P O BOX 12194
RESEARCH TRIANGLE PARK, NC 27709
(ALL CORRES ATTN: SEC OFFICER)
01CY ATTN M SIMONS JR

ROCKWELL INTERNATIONAL CORP.
P O BOX 3105
ANAHEIM, CA 92803
01CY ATTN V DE MARTINO
01CY ATTN V STRAHAN
01CY ATTN G MESSENGER
01CY ATTN J BELL
01CY ATTN T OKI

051 DATE 25/04/80

DEPARTMENT OF DEFENSE CONTRACTORS

ROCKWELL INTERNATIONAL CORP.
SPACE DIVISION
12214 SOUTH LAKEWOOD BOULEVARD
DOWNEY, CA 90241
01CY ATTN D STEVENS

ROCKWELL INTERNATIONAL CORP.
915 LAPHAM STREET
EL SEGUNDO, CA 90245
01CY ATTN TIC BA08
01CY ATTN T YATES

SANDERS ASSOCIATES, INC.
95 CANAL STREET
NASHUA, NH 03060
01CY ATTN L ARCHEUR

SANDIA NATIONAL LABORATORIES
P O BOX 5800
ALBUQUERQUE, NM 87185
(ATTN MAIL SERVICES SECTION FOR INTENDED RECIPIENT
01CY ATTN DOC CON FOR E COPPAGE
01CY ATTN DOC CON FOR W DAWES
01CY ATTN DOC CON FOR R GREGORY
01CY ATTN DOC CON FOR J RAPNUM
01CY ATTN DOC CON FOR J HOOD

SCIENCE APPLICATIONS, INC.
P O BOX 2351
LA JOLLA, CA 92038
01CY ATTN V VERBINSKI
01CY ATTN D LONG
01CY ATTN V ORPHAN
01CY ATTN J NABER

SCIENCE APPLICATIONS, INC.
8400 WESTPARK DRIVE
MCLEAN, VA 22101
01CY ATTN W CHADSEY

SCIENCE APPLICATIONS, INC.
P O BOX 1458
COLORADO SPRINGS, CO 80901
01CY ATTN D STRIBLING

SINGER CO.
1150 MCBRIDE AVENUE
LITTLE FALLS, NY 07424
01CY ATTN J BRINKMAN

SINGER CO.
DATA SYSTEMS
150 TOTOWA ROAD
WAYNE, NJ 07470
01CY ATTN P SPIEGEL

SPERRY RAND CORP.
SPERRY MICROWAVE ELECTRONICS
P O BOX 4648
CLEARWATER, FL 33518
01CY ATTN ENGINEERING LABORATORY

SPERRY RAND CORP.
SPERRY DIVISION
MARCUS AVENUE
GREAT NECK, NY 11020
01CY ATTN E SCARAVAGLIONE
01CY ATTN P MARAFFINO
01CY ATTN C CRAIG
01CY ATTN R VIOLA

SPERRY RAND CORP.
SPERRY FLIGHT SYSTEMS
P O BOX 21111
PHOENIX, AZ 85036
01CY ATTN D SCHOW

SPERRY UNIVAC
UNIVAC PARK
P O BOX 3525
ST PAUL, MN 55165
01CY ATTN J INDA

SPIRE CORP.
P O BOX D
BEDFORD, MA 01730
01CY ATTN R LITTLE

SRI INTERNATIONAL
333 RAVENSWOOD AVENUE
MENLO PARK, CA 94025
01CY ATTN P DOLAN
01CY ATTN B GASTEN
01CY ATTN A WHITSON

DEPARTMENT OF DEFENSE CONTRACTORS

SYSTRON-DONNER CORP.
1090 SAN MIGUEL ROAD
CONCORD, CA 94518
01CY ATTN J INDELICATO

TELEDYNE RYAN AERONAUTICAL
2701 HARBOR DRIVE
SAN DIEGO, CA 92138
01CY ATTN J RAWLINGS

TEXAS INSTRUMENTS, INC.
P O BOX 225474
DALLAS, TX 75265
(UNCLASSIFIED TO P O BOX 6015)
01CY ATTN A PELETIER
01CY ATTN R STEHLIN

TEXAS INSTRUMENTS, INC.
P O BOX 226015
DALLAS, TX 75266
01CY ATTN F POBLENZ

TRW DEFENSE & SPACE SYS GROUP
ONE SPACE PARK
REDONDO BEACH, CA 90278
01CY ATTN A PAVELKO
01CY ATTN A WITTELES
01CY ATTN H HOLLOWAY
01CY ATTN O ADAMS
01CY ATTN R KINGSLAND
01CY ATTN P GUILFOYLE

TRW DEFENSE & SPACE SYS GROUP
P O BOX 1310
SAN BERNARDINO, CA 92402
01CY ATTN R KITTER
01CY ATTN F FAY
01CY ATTN M GORMAN
01CY ATTN ATTN W WILLIS

TRW SYSTEMS AND ENERGY
P O BOX 368
CLEARFIELD, UT 84015
01CY ATTN G SPEHAR
01CY ATTN R GILILLAND

VOUGHT CORP.
P O BOX 225907
DALLAS, TX 75265
(FORMERLY LTV AEROSPACE CORPORATION)
01CY ATTN R TOMME
01CY ATTN LIBRARY
01CY ATTN TECHNICAL DATA CENTER

WESTINGHOUSE ELECTRIC CO.
AEROSPACE & ELECTRONIC SYSTEMS DIV
P O BOX 1693
BALTIMORE-WASHINGTON INTL AIRPORT
BALTIMORE, MD 21203
01CY ATTN L MCPHERSON

WESTINGHOUSE ELECTRIC CORP.
DEFENSE AND ELECTRONIC SYSTEMS CTR
P O BOX 1693
BALTIMORE-WASHINGTON INTL AIRPORT
BALTIMORE, MD 21203
01CY ATTN D CRICHI
01CY ATTN H KALAPACA


END
DATE
FILMED
3-82
DTIC